NACA RM L53F22a

NACA

RESEARCH MEMORANDUM

A TRANSONIC WIND-TUNNEL INVESTIGATION OF THE EFFECTS OF NACELLES ON THE AERODYNAMIC CHARACTERISTICS OF A COMPLETE MODEL CONFIGURATION

By Melvin M. Carmel and Thomas L. Fischetti

Langley Aeronautical Laboratory
Langley Field, Va.

NATIONAL ADVISORY COMMITTEE
FOR AERONAUTICS

WASHINGTON
September 22, 1953
Declassified March 18, 1960

NACA RM L53F22a

NATIONAL ADVISORY COMMITTEE FOR AERONAUTICS

RESEARCH MEMORANDUM

A TRANSONIC WIND-TUNNEL INVESTIGATION OF THE EFFECTS OF NACELLES ON THE AERODYNAMIC CHARACTERISTICS OF A COMPLETE MODEL CONFIGURATION

By Melvin M. Carmel and Thomas L. Fischetti

SUMMARY

Comparisons have been made of the aerodynamic characteristics of a model configuration having a wing of aspect ratio 3.5, taper ratio 0.2, thickness ratio 5.5 percent, and 47° sweepback of the quarter-chord line in combination with three basic types of nacelles, buried nacelles, pylon-suspended nacelles, and underslung nacelles, at various wing spanwise locations. The results were obtained in the Langley 8-foot transonic tunnel for Mach numbers from 0.70 to 1.12. The angle-of-attack range generally varied from -6° to 8°, but in some instances the range was extended to 16°. Reynolds number, based on the wing mean aerodynamic chord, varied from 2.60×10^6 to 2.95×10^6.

The comparisons show that the configuration with the nacelles buried in the wing root has the least drag and best performance characteristics of any of the nacelle configurations throughout the test Mach number range. The lowest drag-rise increment near the speed of sound at zero lift was obtained for the model configuration with nacelles that had the least maximum total cross-sectional area and the most gradual rate of axial development of total cross-sectional area. Outboard movement of the nacelle location leads to delays in the lift coefficient at which pitch-up occurs in the subsonic Mach number range.

Addition of nacelles to the configuration has, in general, only small effects on the variation of lift-curve slope or aerodynamic-center position with Mach number at lift coefficients between 0 and 0.3.

INTRODUCTION

Investigations have been conducted in the Langley 8-foot transonic tunnel on the aerodynamic characteristics of a complete model configuration having a wing of aspect ratio 3.5, taper ratio 0.2, and thickness ratio 5.5 percent with 47° sweepback of the quarter-chord line. The mode configuration was tested in conjunction with several nacelles which involved variation in type of nacelle and nacelle location.

The nacelle configurations investigated consist of pylon-suspended and underslung nacelles located at various spanwise positions on the wing and buried nacelles located in the wing root. The effect of two nacelle nose shapes was also investigated. The results presented herein consist of lift, drag, and pitching-moment characteristics obtained at Mach numbers from 0.70 to 1.12. The angles of attack generally varied from -6° to 8°, but in some instances this range was extended to 16°.

The Reynolds number, based on the wing mean aerodynamic chord, varied from 2.60×10^6 to 2.95×10^6.

SYMBOLS

A_1	inlet area of one nacelle, sq in.
b	wing span, in.
c	pylon chord, in.
$\bar{c}$	mean aerodynamic chord, in.
C_D	drag coefficient, measured drag coefficient minus base pressure-drag coefficient
ΔC_D	incremental drag coefficient added by nacelle
ΔC_{D_0}	incremental drag rise at zero lift, $\Delta C_{D_0} = C_{D_{0_M}} - C_{D_{0_{M=0.85}}}$
$C_{D_{int}}$	internal-drag coefficient based on wing area
C_L	lift coefficient
C_M	pitching-moment coefficient about the 0.35 point of the mean aerodynamic chord

$dC_L/d\alpha$ lift-curve slope

dC_M/dC_L pitching-moment-curve slope

$(L/D)_{max}$ maximum lift-drag ratio

M Mach number

m mass-flow rate, slugs/sec

t pylon ordinate

V_o free-stream velocity, ft/sec

X pylon station

α angle of attack, deg

ρ_o free-stream density, slugs/cu ft

Model designations:

N pylon-suspended dual nacelles, conical nose, located at 50 percent wing semispan

N_2 buried nacelles, located at wing root

N_3 pylon-suspended dual nacelles, wedge nose, located at 60 percent wing semispan

N_4 pylon-suspended dual nacelles, wedge nose, located at 50 percent wing semispan

N_5 underslung single nacelles, conical nose, located at 40 and 70 percent wing semispan

N_6 underslung dual nacelles, wedge nose, located at 50 percent wing semispan

APPARATUS AND METHODS

Tunnel

The tests were conducted in the Langley 8-foot transonic tunnel which is a single-return wind tunnel having a dodecagonal, slotted test

section. This tunnel is designed to obtain aerodynamic data through the speed of sound without the usual effects of choking and blockage. The tunnel operates at atmospheric stagnation pressures.

Configurations

The model used for this test is shown in figure 1. Geometric characteristics of the model are given in table I.

Three basic types of nacelles were tested on the basic model; namely, the buried nacelle, the pylon-suspended nacelle, and the underslung nacelle. Details of the nacelles are given in figures 2 to 6. Pertinent information on the various nacelles tested is given in the following table:

Configuration	Nacelle installation	Type	Location	Nose inlet	A_1, sq in.
N	Pylon-suspended	Dual unit	0.50b/2	Conical	0.316
N_2	Buried	Dual unit	Wing root	Wing root leading edge	.349
N_3	Pylon-suspended	Dual unit	0.60b/2	Wedge	.327
N_4	Pylon-suspended	Dual unit	0.50b/2	Wedge	.327
N_5	Underslung	Single unit	0.40 and 0.70b/2	Conical	.316
N_6	Underslung	Dual unit	0.50b/2	Wedge	.327

The buried nacelle installation N_2 shown in figure 2 had a wing root inlet which was divided into two passages each leading to a circular exit behind the trailing edge of the wing. To provide for the installation of this nacelle, the inboard sections of the basic wing were thickened by the addition of a plate on the lower surface. All of the pylon-suspended dual nacelles had separate intakes and ducts. The same pylons were used for all pylon-suspended-nacelle tests and the leading edge was swept forward 66.2°. Ordinates for the pylon are given in table II. A photograph of the pylon-suspended, dual-unit, wedge-nose configuration N_4 is presented in figure 4, and details of the underslung, single-unit, conical-nose nacelles are presented in figure 5.

The two nose shapes investigated consisted of a wedge-shape inlet and a conical-shape inlet. Details of the wedge-shape inlet are given in figure 6. Complete details of the internal ordinates of the conical-shape inlet are lacking; however, some details are given in figure 3. The inlet areas of each nacelle (which in all cases was the minimum area) are given in the table above.

Model Support System

The model was attached to a sting support system by means of an internal, six-component, electrical strain-gage balance. The angle of attack was varied by pivoting the sting support downstream of the model. By inserting couplings upstream of the pivot point, the model was kept near the center of the tunnel throughout the entire angle range tested. The angle-of-attack mechanism was remotely controlled so that angle-of-attack changes could be made while the tunnel was operating.

Measurements and Accuracy

The average free-stream Mach number was determined to within ±0.003 from a calibration with respect to the pressure in the chamber surrounding the slotted test section.

The measured lift, drag, and pitching-moment coefficients had an accuracy, based on balance design and repeatability of data, of ±0.003, ±0.0015, and ±0.003, respectively. Measurements were made over a Mach number range of 0.70 to 1.12 with angles of attack that generally varied from -6° to 8° but which were extended in some cases to 16°.

The angle of attack of the model was measured with a calibrated, pendulum-type inclinometer located within the sting downstream of the model. The accuracy of this device was $\pm 0.10^\circ$ at all test Mach numbers.

Base pressures were measured at points on the periphery of the sting just inside of the model base. The drag data for these tests have been corrected to values that would have been obtained had the entire base of the body been subject to free-stream static pressure. No corrections, however, have been made to the data for the interference effects of the sting support system.

Reference 1 indicates that above a Mach number of 1.00, the data are affected by reflected shock waves off the tunnel walls. Up to a Mach number of 1.03, however, the effect of these disturbances was found to be small. The extent to which the data for this test are affected at Mach numbers above 1.03 is not known. It is believed that

the effects of shock reflection on lift coefficient are small. It would be expected that shock reflection would have an effect on pitching-moment and drag results above a Mach number of 1.03; however, an inspection of the data indicates that the shock-reflection effects on these data are small. Similar studies without a tail (ref. 2) have shown small effects of shock reflection in this speed range.

RESULTS

The reference axes of the data presented in the figures have been changed from body axes to wind axes. All references to nacelles in the following discussion pertain to data presented for nacelles plus basic configuration. The lift-curve and pitching-moment-curve slopes were obtained from straight lines averaging that portion of the curves between a lift coefficient of 0 and 0.3. The pitching moments are taken about the 0.35 point of the mean aerodynamic chord.

The basic aerodynamic characteristics - angle of attack, drag coefficient, and pitching-moment coefficient plotted against lift coefficient - for the basic configuration and the nacelle configurations investigated are presented in figures 7 to 13. Figure 14 shows the axial distribution of total cross-sectional area for the basic configuration and for all the nacelle configurations. For the nacelle configurations, the total cross-sectional area was reduced to allow for the mass flow through the nacelles. This was done by computing the mass flow through the nacelles for a Mach number of 1.00 and converting it to an equivalent free-stream area. Figures 15, 16, and 17 show a comparison of the drag characteristics, drag-rise characteristics, and maximum lift-drag ratios, respectively, for the various nacelle configurations tested. A comparison of the drag due to lift for the various nacelle configurations is given in figure 18. Figures 19 and 20 show the effect of nacelle nose shape on incremental drag coefficient and maximum lift-drag ratio, respectively. A comparison of the lift-curve slopes and pitching-moment-curve slopes for the various nacelle configurations tested are presented in figures 21 and 22, respectively. The lift coefficient at which pitch-up occurs is presented for the various nacelle configurations in figure 23.

Internal drag was measured for three of the nacelles N, N_2, and N_4, and although it was of significant magnitude, the differences between any of the nacelles were found to be small. The internal drag of the nacelles was therefore not removed from the total drag of the nacelle configurations as it would have little effect on the comparisons made. The method for obtaining internal drag is presented in the appendix. Values of internal-drag coefficient for three of the nacelle configurations tested are presented in figure 24 as a

function of lift coefficient for several Mach numbers. This drag coefficient is the total value for four nacelles of a given nacelle configuration. Mass-flow characteristics for three of the nacelle configurations are presented in figure 25.

DISCUSSION

A Study of the Drag Characteristics of the Various Nacelle Configurations

A comparison of the drag characteristics for the nacelle configurations tested is presented in figure 15 for lift coefficients of 0, 0.3, and 0.5. The drag characteristics for nacelle configuration N are not included but are discussed in a later section. For comparative purposes, the drag characteristics for the basic configuration are also included as part of figure 15.

For the zero-lift condition, adding any of the test nacelles to the basic configuration increases the drag coefficient at all test Mach numbers. It may be noted from figure 15 that near the speed of sound and up to the highest test Mach number, the differences in drag coefficient between any of the nacelle configurations and the basic configuration are considerably greater than at low speeds. Adding the buried nacelles N_2 to the basic configuration increases the drag coefficient the least of any of the nacelles. For example, at a Mach number of 1.00, the buried nacelles N_2 add 21 percent to the drag coefficient for the basic configuration, whereas the underslung nacelles N_6 add 100 percent to that for the basic configuration. It must be remembered that the internal drag was not subtracted from the total drag of the nacelle configurations. Had it been subtracted, the drag of the N_2 configuration would have been about the same as that for the basic configuration (indicating a favorable interference) and the drag of the N_6 configuration would have been about 80 percent greater than that for the basic configuration. The adverse effects of the other nacelles on the basic drag coefficient when compared with those of the buried nacelles near the speed of sound at zero lift may be explained primarily on the basis of the transonic drag-rise rule discussed in reference 3.

The transonic drag-rise rule states that the drag rise of thin, low-aspect-ratio wing-body combinations near the speed of sound at zero lift is primarily dependent upon the rate of axial development of total cross-sectional area. It may be noted from figure 14 that the maximum cross-sectional area of the configuration N_2 is not only much less than for the other nacelle configurations, but its rate of axial development is more gradual. In accordance with the transonic drag-rise rule, this should lead to a lower drag rise for the N_2 configuration than for any

of the other nacelle configurations near the speed of sound at zero lift. The incremental drag-rise curves for the various nacelles at zero lift (fig. 16) show that the buried nacelle configuration has the least drag rise near a Mach number of 1.00 of any of the nacelle configurations. These curves were started at a Mach number of 0.85 in order to minimize any skin-friction effects. It may also be noted that the drag rise near a Mach number of 1.00 for the nacelle configurations becomes increasingly greater as their maximum cross-sectional areas become larger, especially when this occurs with a more rapid development of cross-sectional area. (See figs. 14 and 16.)

One point that can be seen from the data is that nacelle configuration N_4 has slightly lower drag coefficients at zero lift near the speed of sound than nacelle configuration N_3 even though the nacelles are the same size (fig. 16). This results from the fact that the nacelles are placed at different spanwise positions which leads to a different axial location for the nacelles, so that the axial development of cross-sectional area is slightly more favorable for the configuration with nacelle N_4. Likewise, the total volumes of underslung nacelles N_5 and N_6 are approximately the same; however, the separated nacelle configuration N_5 has the lesser maximum area and the more gradual axial development of cross-sectional area of these two nacelle configurations. Therefore it would be expected that N_5 would have a lower drag rise than N_6 near the speed of sound at zero lift and this was confirmed by the data (fig. 16). These results with regard to the transonic drag-rise rule have been substantiated by tests on other wing-body combinations with nacelles tested by the rocket technique (ref. 4), thus showing that the area rule may be extended to encompass nacelles as well as wing-body combinations alone.

It is obvious from the preceding discussion that the transonic drag-rise rule is a rational means of qualitatively determining the interference effects and drag-rise characteristics of aircraft configurations at zero lift and it has been shown that for minimum drag rise near the speed of sound, nacelles should be added in such a way that the maximum total cross-sectional area is kept as small as possible and the axial development of the cross-sectional area should be made as gradual as possible.

In order to determine how much of the drag added to the basic configuration by the nacelles was interference drag, the drag of the basic configuration was subtracted from that for the configuration with nacelles for several nacelle configurations. A comparison (unpresented) was then made between these nacelle plus interference drags and the drags obtained for similar isolated nacelles from rocket test data. The results indicate that no unfavorable interference drag was produced by the separated underslung nacelle configuration N_5 at any of the test

Mach numbers. The greatest interference drag was produced by the underslung dual nacelle configuration N_6 and the pylon-suspended nacelles N_3. This interference drag, near a Mach number of 1.00, amounted to about as much as the drag for a comparable isolated nacelle. The interference drags for the nacelles of the present investigation have been found to be comparable with those of tests with similar nacelle configurations (see ref. 5). This indicates, therefore, that with proper nacelle positioning the drag of the various nacelles on the basic configuration at zero-lift conditions can be reduced by reducing the interference drag.

At lift coefficients of 0.3 and 0.5, the same general trends may be found that exist at a lift coefficient of zero; that is, the buried nacelle configuration has the lowest drag coefficients throughout the test Mach number range and the least drag rise near the speed of sound of any of the nacelle configurations tested (fig. 15).

A comparison of the effects of the various nacelle configurations on maximum lift-drag ratio is presented in figure 17. The buried nacelle configuration has considerably higher maximum lift-drag ratios throughout the Mach number range than any of the other nacelle configurations tested. A comparison of the drag due to lift for the various nacelle configurations is given in figure 18. A study of figures 16 and 18 shows that the higher maximum lift-drag ratios for the buried nacelle configurations are primarily due to the influence of the drag at zero lift rather than the drag due to lift.

The incremental drag and maximum lift-drag ratios, figures 19 and 20, respectively, for the pylon-suspended nacelles N and N_4, which differ only in nose shape, are only slightly different for the conical-nose N and the wedge-nose N_4 nacelle configurations.

Stability Characteristics

It may be seen from figure 21 that the addition of the nacelles to the basic configuration has, in general, little effect on the variation of lift-curve slope with Mach number. The buried nacelle configuration, however, has slightly greater lift-curve slopes throughout most of the test Mach number range than do the basic or other nacelle configurations.

The general shapes of the slope of the pitching-moment curves with Mach number are about the same for the basic configuration and for the nacelle configurations (fig. 22). Addition of the nacelles, however, has a destabilizing effect inasmuch as the aerodynamic-center position is moved forward, generally, from 2 percent to 6 percent at low speeds and as much as 10 percent at supersonic speeds.

A comparison of the pitching-moment curves for the basic configuration and the various nacelle configurations indicated that a pitch-up instability existed. Figure 23 presents the lift coefficient at which pitch-up occurs for the basic and nacelle configurations. This figure shows that, for pylon-suspended nacelles N_3 and N_4 at Mach numbers to about 0.94, positioning the nacelles farther outboard on the wing delays the lift coefficient at which pitch-up occurs by as much as 0.50. A comparison between underslung nacelles N_5 and N_6 at Mach numbers to about 0.94 shows that separating the dual-unit nacelles and moving the average distance between the nacelles and the plane of symmetry to a position farther outboard on the wing delays the lift coefficient at which pitch-up occurs by as much as 0.30. This delay in lift coefficient for pitch-up for the latter nacelles is not so large as that experienced with the pylon-suspended nacelles. At Mach numbers above 0.95, addition of nacelles to the basic configuration has only a small effect on the lift coefficient at which pitch-up occurs. It may be noted from figure 23 that there still exists a serious longitudinal stability problem in the lower transonic range near 0.95.

CONCLUSIONS

Tests have been performed to determine the effects of various types of nacelles tested in combination with a complete model configuration with primary emphasis placed on drag and performance characteristics. The results of these tests lead to the following conclusions:

1. The configuration with the nacelles buried in the wing root has the lowest drag and best performance characteristics of any of the nacelle configurations throughout the test Mach number range.

2. The lowest drag-rise increment near the speed of sound at zero lifting conditions was obtained for the model configuration with nacelles that had the least maximum total cross-sectional area and the most gradual rate of axial development of total cross-sectional area.

3. Outboard movement of the nacelle location leads to delays in the lift coefficient at which pitch-up occurs in the subsonic Mach number range.

4. Addition of nacelles to the configuration has, in general, only small effects on the variation of lift-curve and pitching-moment-curve slopes with Mach number at lift coefficients between 0 and 0.3.

Langley Aeronautical Laboratory,
National Advisory Committee for Aeronautics,
Langley Field, Va., June 10, 1953.

APPENDIX

METHOD FOR OBTAINING INTERNAL DRAG

Several assumptions must be made before the two static orifices which were installed in the nacelle ducts can be used to compute the internal drag. The stagnation pressure and temperature must be assumed to be the same at the two stations, and the flow across the duct must be assumed to be uniform. The latter assumption appears to be the more questionable, particularly at angles of attack. It should be remembered, however, that the errors which may be introduced by the above assumptions will have only a minor influence on the external drag of the basic model with nacelles because the absolute magnitude of the internal drag is small.

The internal drag D_{int} is defined as

$$D_{int} = A_e(p_o - p_e) + m_e(V_o - V_e)$$

where

A duct area

p static pressure

V velocity

$m = \rho AV$

ρ density

Symbols with subscript e refer to duct exit conditions and symbols with subscript o refer to free-stream conditions.

By using the assumptions discussed above, the following equation for the internal-drag coefficient of each nacelle duct can be derived:

$$C_D = \frac{2}{\gamma M_o^2}\frac{A_e}{S}\left\{1 - \frac{p_e}{p_o} + \frac{p_e}{p_o}\gamma M_e^2\left[\frac{M_o}{M_e}\left(\frac{1 + \frac{\gamma - 1}{2}M_e^2}{1 + \frac{\gamma - 1}{2}M_o^2}\right)^{1/2} - 1\right]\right\}$$

where γ is the ratio of the specific heats, which is 1.40 for air.

REFERENCES

1. Ritchie, Virgil S., and Pearson, Albin O.: Calibration of the Slotted Test Section of the Langley 8-Foot Transonic Tunnel and Preliminary Experimental Investigation of Boundary-Reflected Disturbances. NACA RM L51K14, 1952.

2. Whitcomb, Charles F., and Osborne, Robert S.: An Experimental Investigation of Boundary Interference on Force and Moment Characteristics of Lifting Models in the Langley 16- and 8-Foot Transonic Tunnels. NACA RM L52L29, 1953.

3. Whitcomb, Richard T.: A Study of the Zero-Lift Drag-Rise Characteristics of Wing-Body Combinations Near the Speed of Sound. NACA RM L52H08, 1952.

4. Hoffman, Sherwood, and Pepper, William B., Jr.: The Effect of Nacelle Combinations and Size on the Zero-Lift Drag of a 45° Sweptback Wing and Body Combination as Determined by Free-Flight Tests at Mach Numbers Between 0.8 and 1.3. NACA RM L53E25, 1953.

5. Bielat, Ralph P., and Harrison, Daniel E.: A Transonic Wind-Tunnel Investigation of the Effects of Nacelle Shape and Position on the Aerodynamic Characteristics of Two 47° Sweptback Wing-Body Configurations. NACA RM L52G02, 1952.

TABLE I.- GEOMETRIC CHARACTERISTICS OF MODEL

Wing:	
Area, including area blanketed by fuselage, sq ft	1.367
Aspect ratio	3.5
Taper ratio	0.2
Streamwise thickness, percent chord	5.5
Twist (linear variation from root to tip):	
Root, deg	0
Tip, deg	2.5 washout
Incidence, deg	4
Sweepback of quarter-chord line, deg	47
Horizontal tail:	
Area, including area blanketed by fuselage, sq ft	0.191
Aspect ratio	3.65
Taper ratio	0.2
Streamwise thickness, percent chord	5.5
Incidence, deg	-0.1
Sweepback of quarter-chord line, deg	47
Elevator setting, deg	0
Vertical tail:	
Area (exposed), sq ft	0.121
Aspect ratio (based on exposed span and area)	1.5
Taper ratio	0.2
Streamwise thickness, percent chord	5.5
Sweepback of quarter-chord line, deg	47

TABLE II.- PYLON ORDINATES

X/c	t/c
0	0
.0050	.0040
.0075	.0048
.0125	.0060
.025	.0079
.050	.0109
.075	.0132
.100	.0152
.200	.0207
.300	.0238
.400	.0250
.500	.0241
.600	.0210
.700	.0162
(a)	(a)
1.000	0

[a]Straight-line fairing.

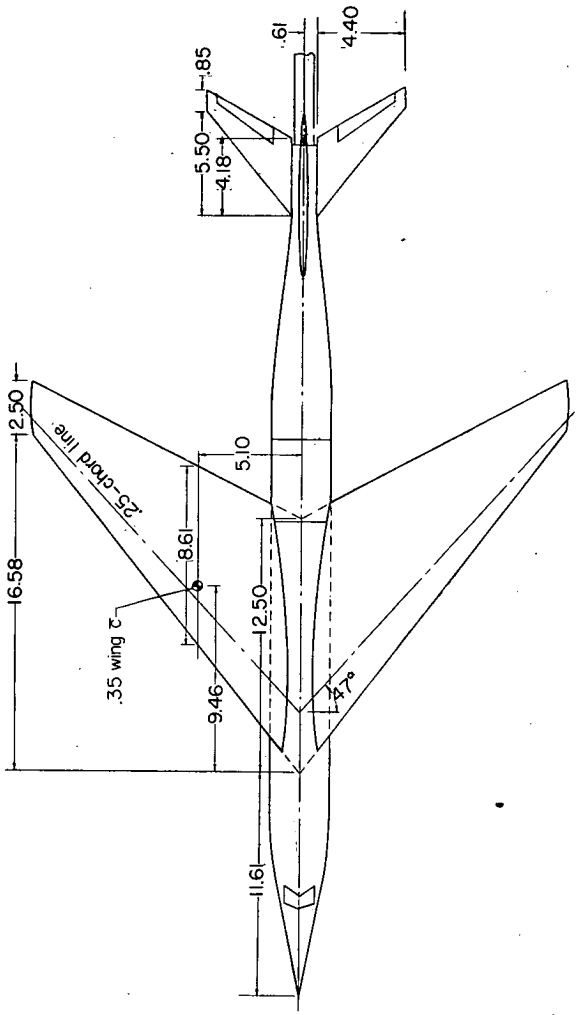

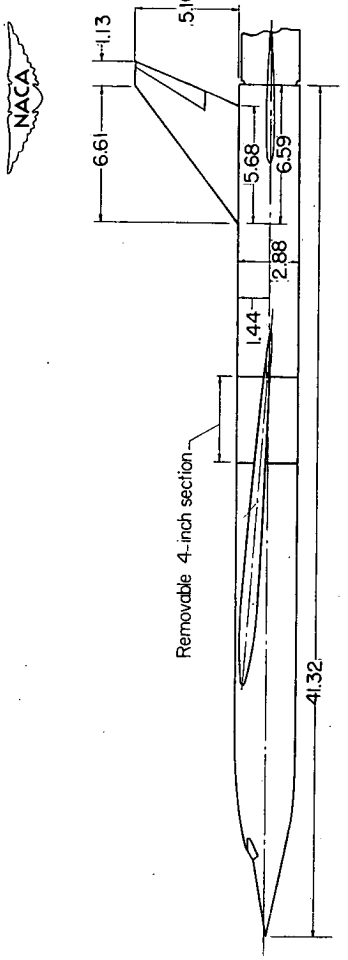

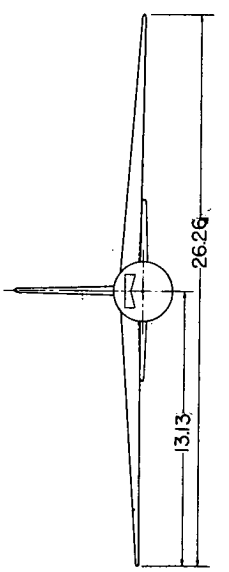

Figure 1.- Details of test model. All dimensions in inches. (Model characteristics are presented in table I.)

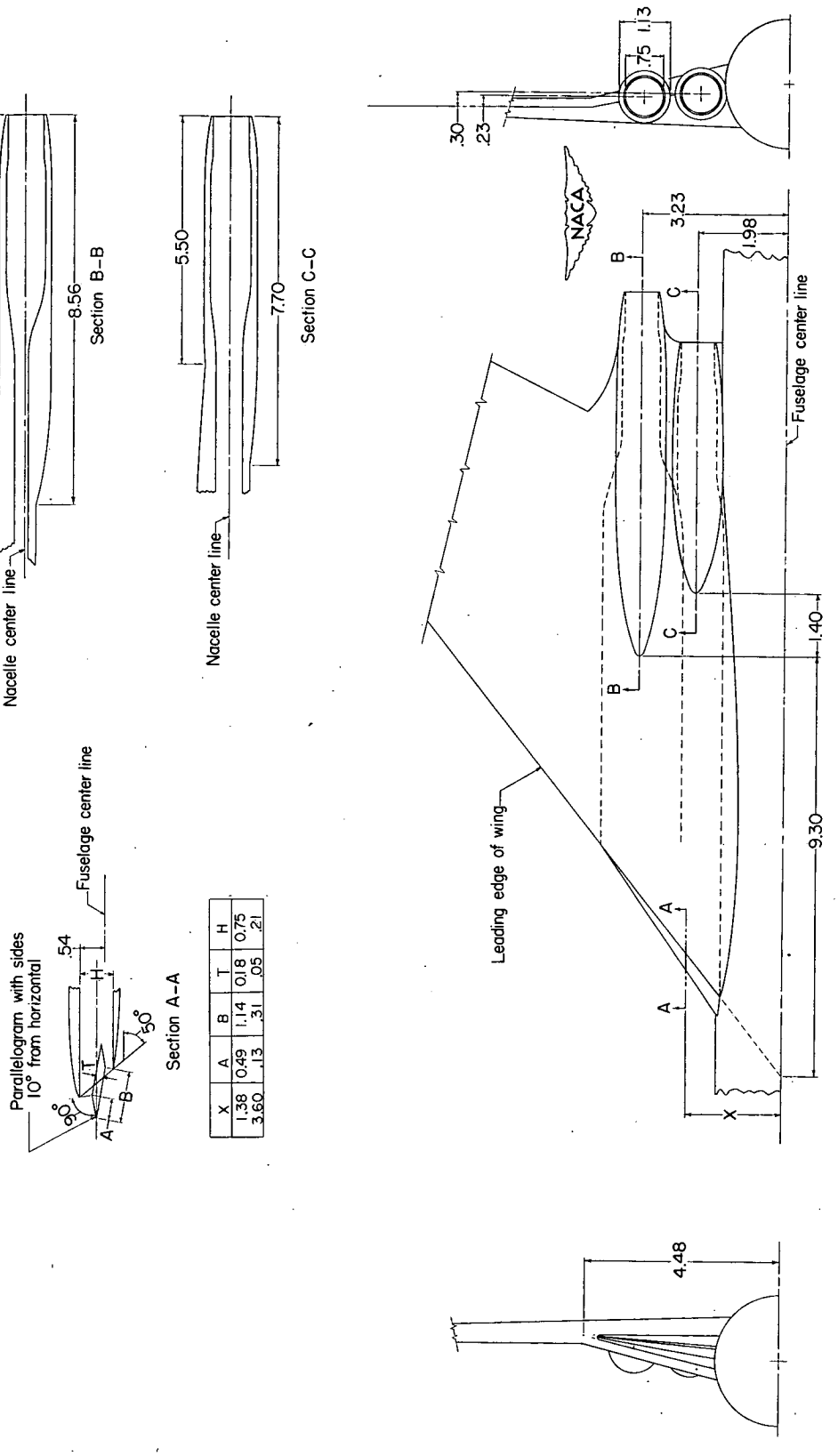

Figure 2.- Details of the buried nacelles N_2. All dimensions in inches.

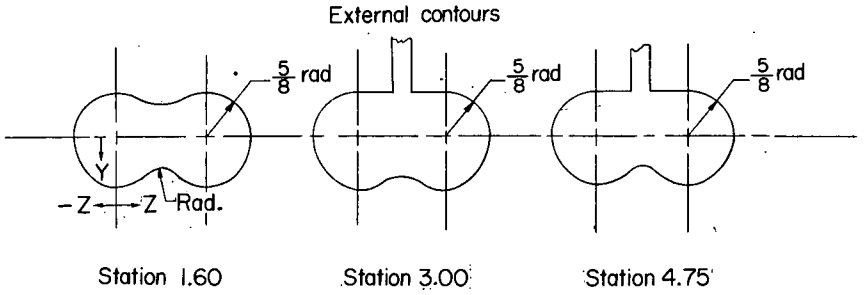

Nacelle external coordinates			
Z	Station		
	1.60	3.00	4.75
	Y	Y	Y
-0.40	0.48	0.52	0.46
-.20	.65	.66	.62
0	.70	.75	.67
.20	.66	.70	.63
.40	.52	.57	.54
.58	.42	.52	.49
Radius	0.19	0.38	0.44

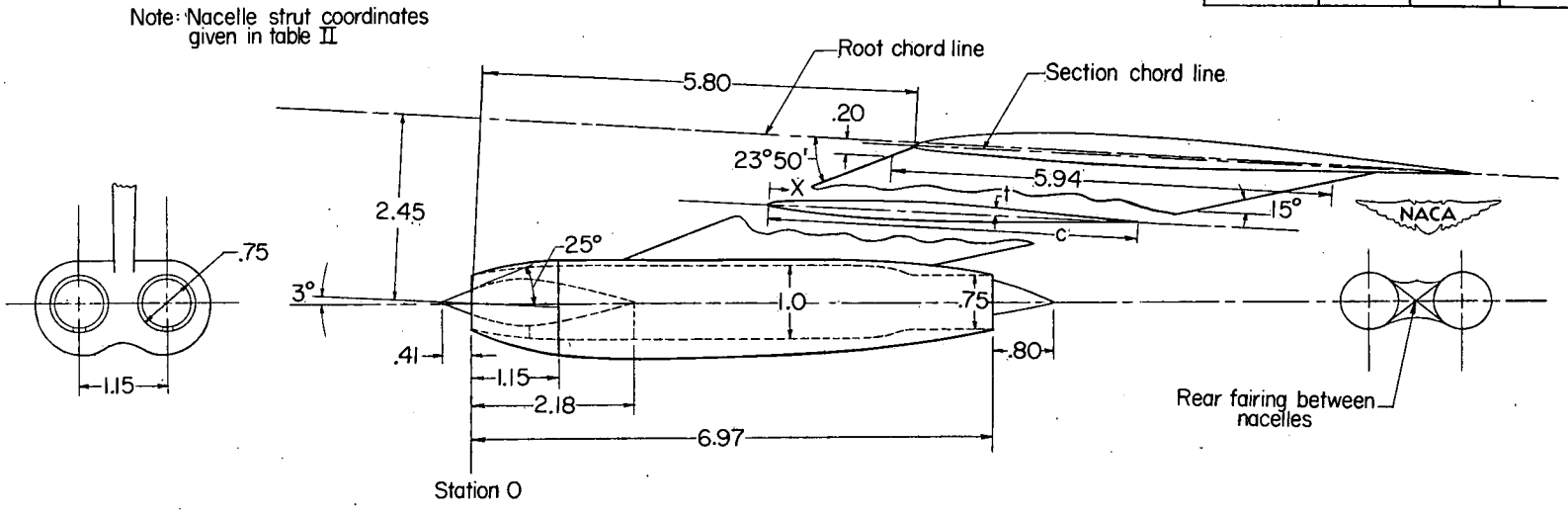

Figure 3.- Details of the pylon-suspended, dual-unit, conical-nose nacelles N. All dimensions in inches.

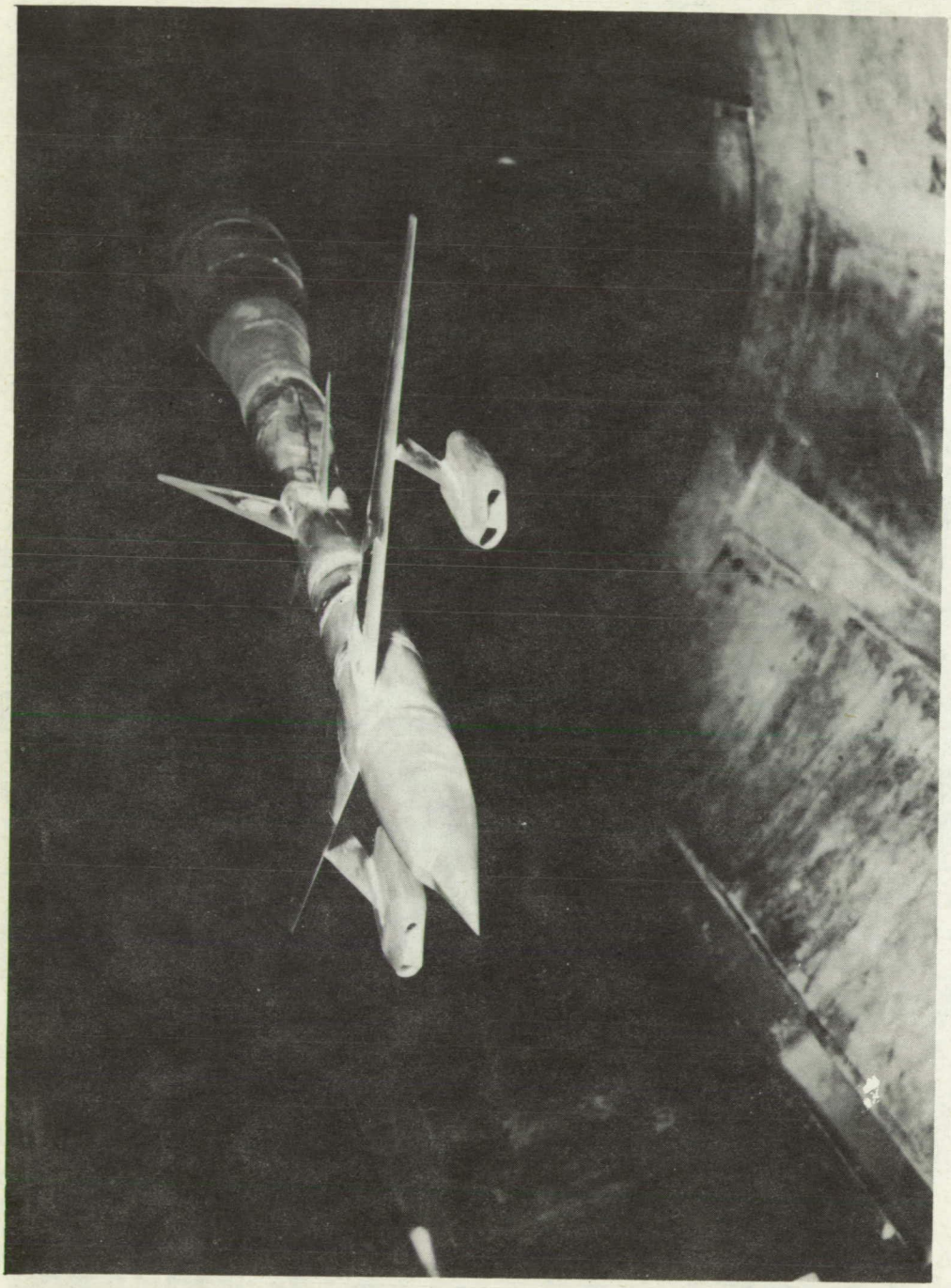

L-73954

Figure 4.- Pylon-suspended, dual-unit, wedge-nose configuration N_4.

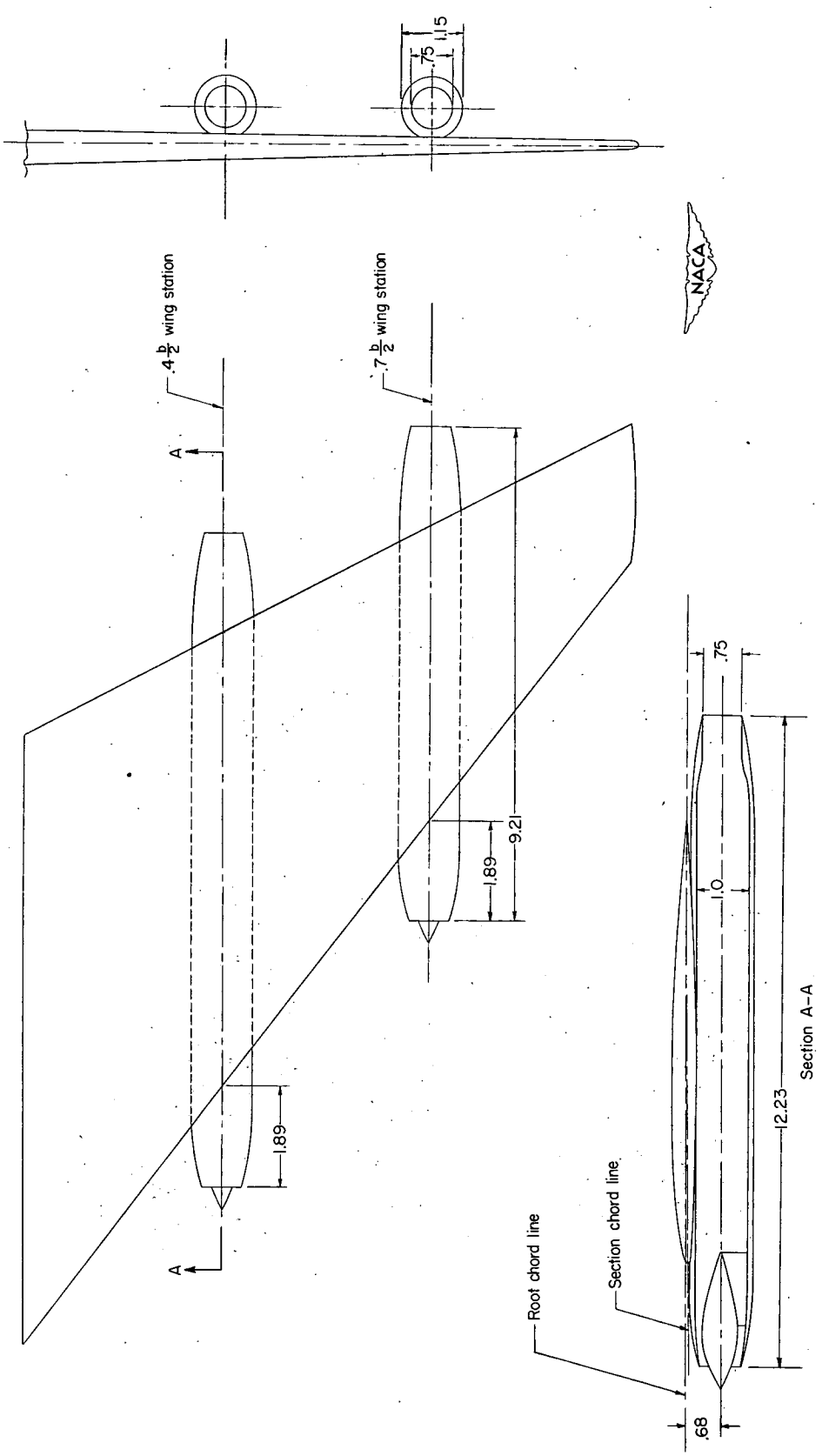

Figure 5.- Details of the underslung, single-unit, conical-nose nacelles N5. All dimensions in inches.

Wedge-nose coordinates			
Station	r	R_1	R_2
1.055	0.186	0.276	0.281
1.510	.250	.350	.379
1.760	.250	.390	.433
2.010	.250	.430	.486
2.260	.250	.469	.538
2.510	.250	.490	.561
2.820	.160	.500	.575

Note: Nacelle center line parallel to wing-root plane

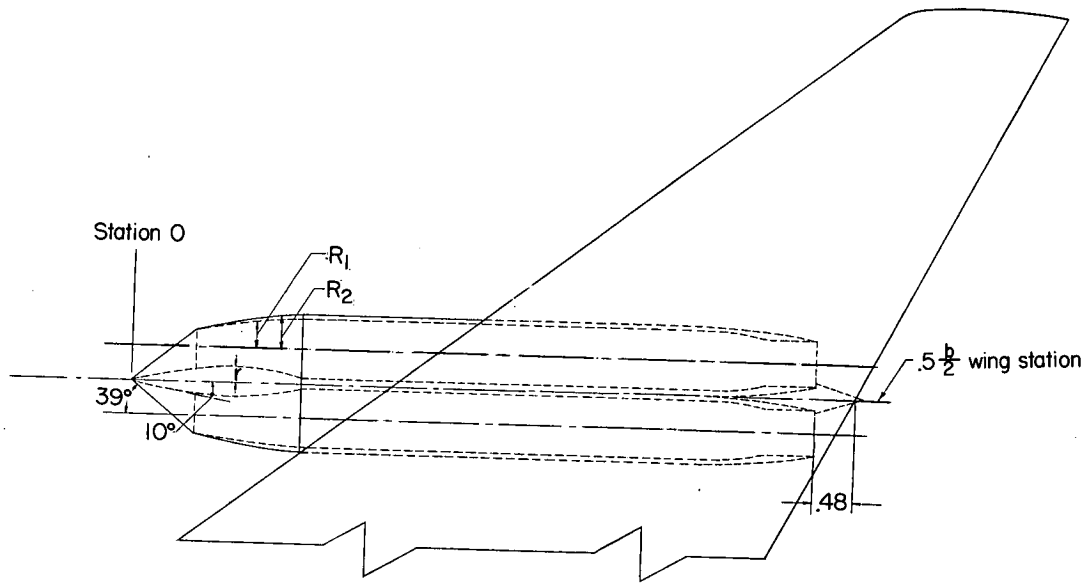

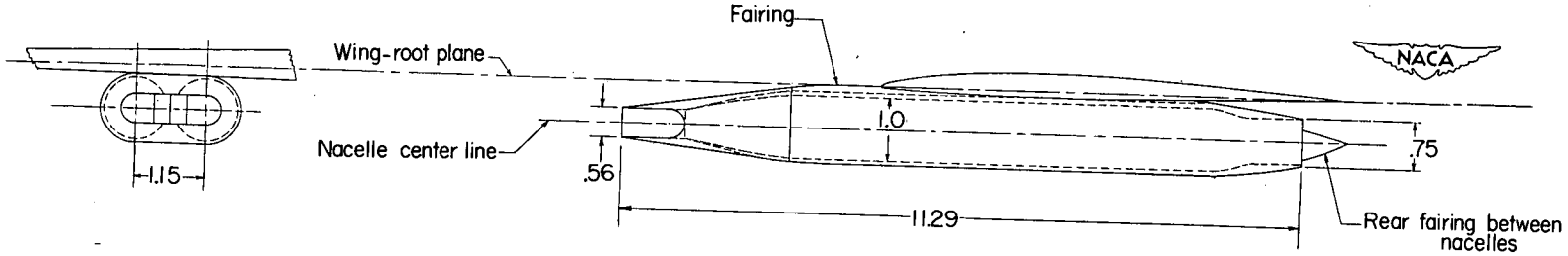

Figure 6.- Details of the underslung, dual-unit, wedge-nose nacelles N_6. All dimensions in inches.

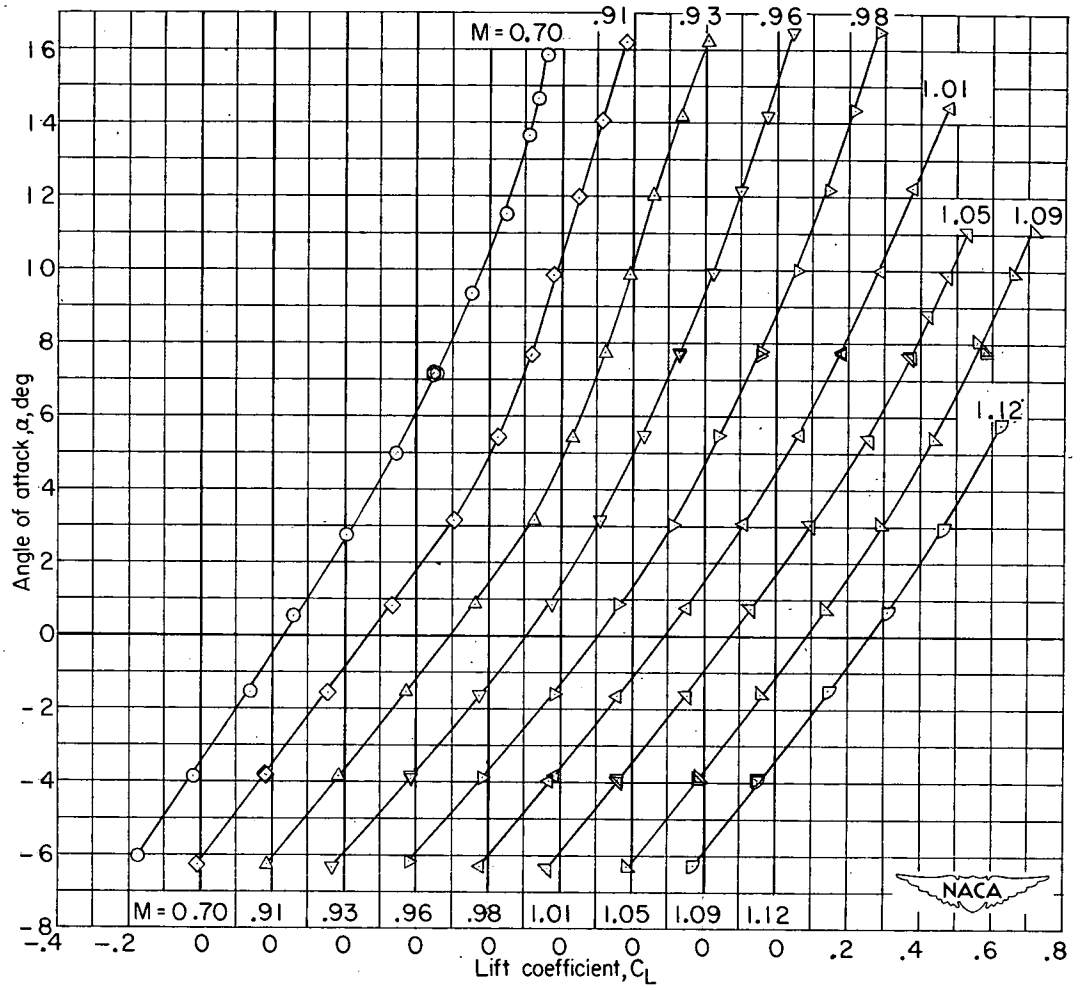

(a) Angle of attack.

Figure 7.- Variation with lift coefficient of the aerodynamic characteristics of the basic configuration.

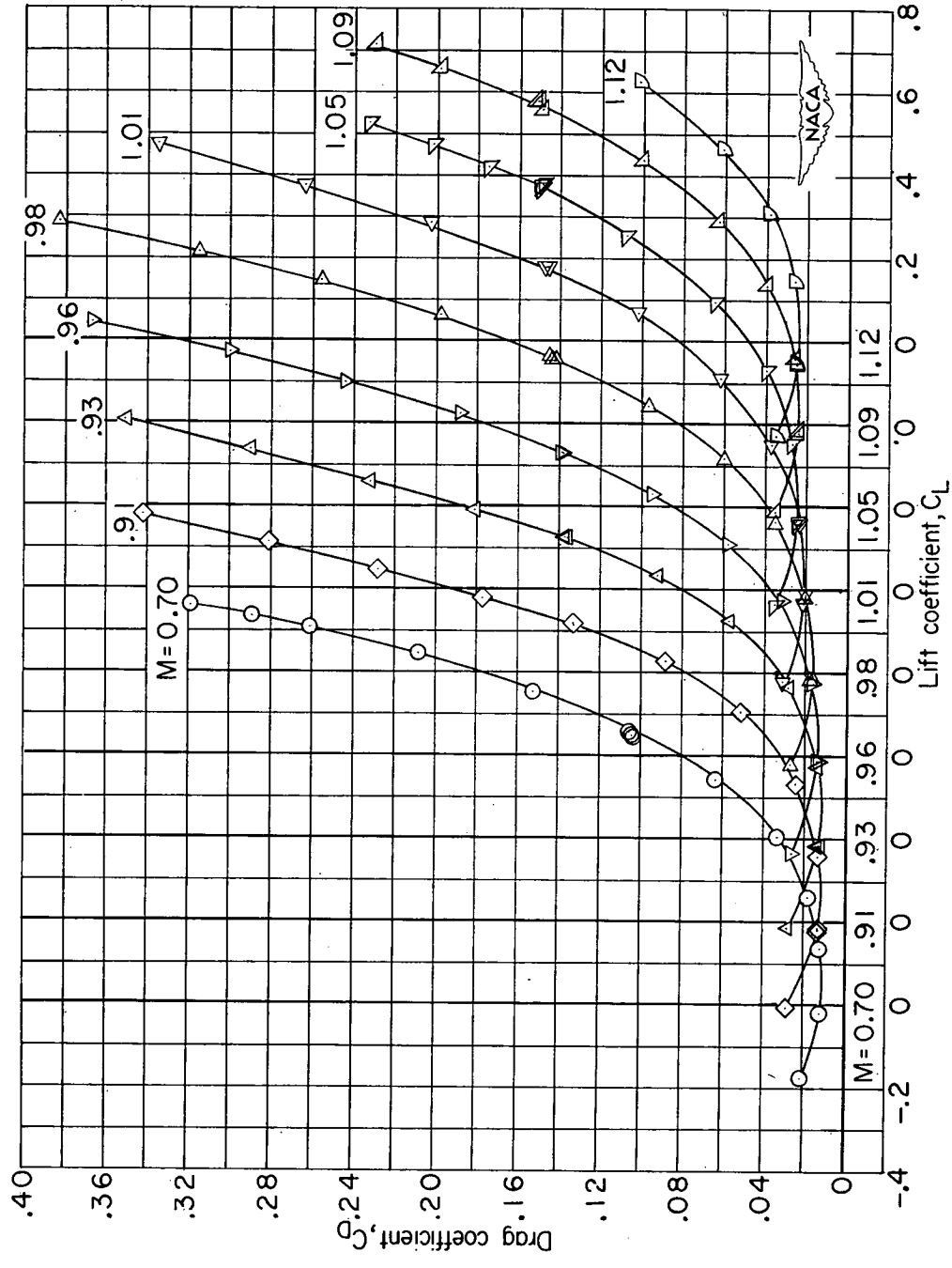

(b) Drag coefficient.

Figure 7.- Continued.

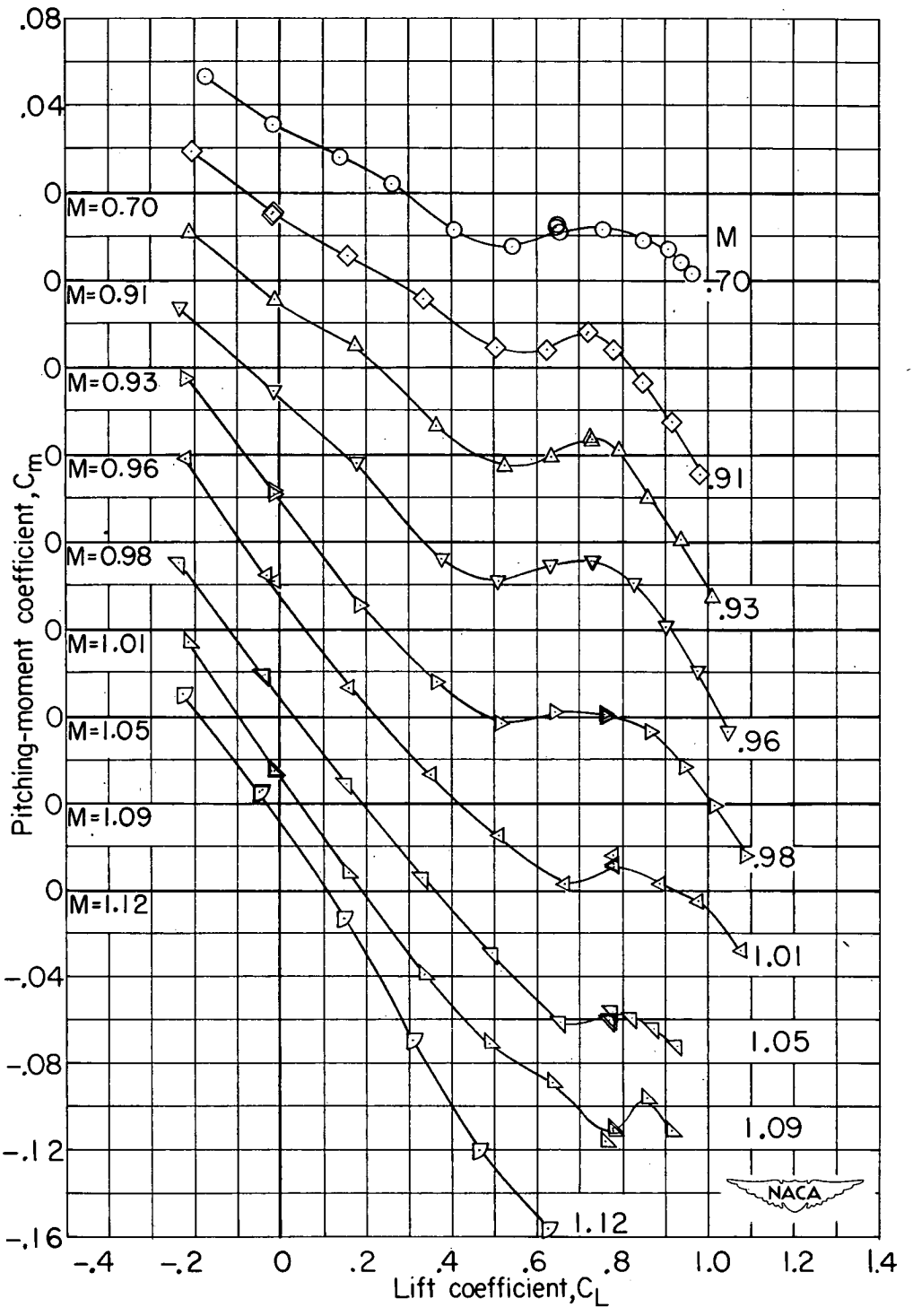

(c) Pitching-moment coefficient.

Figure 7.- Concluded.

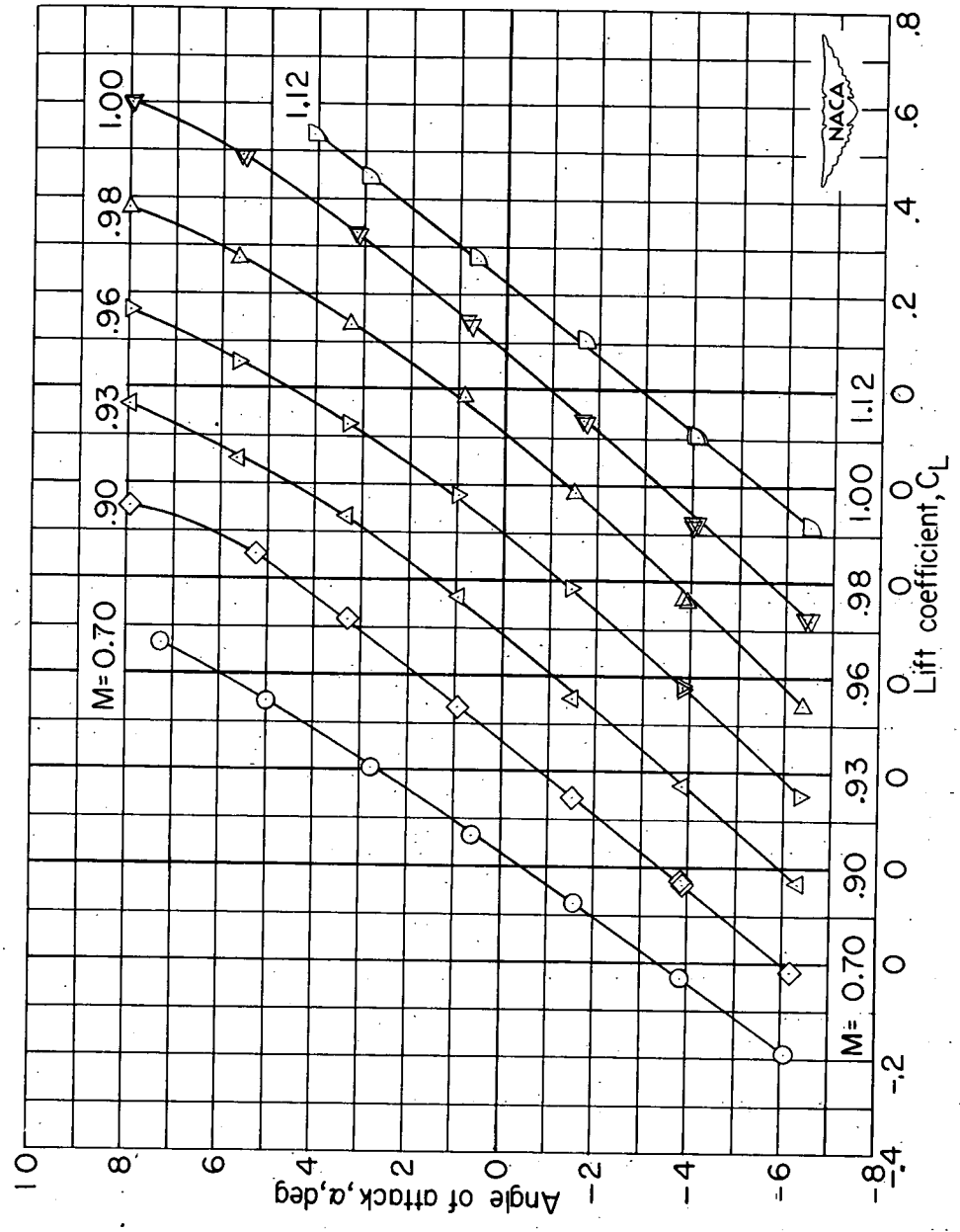

(a) Angle of attack.

Figure 8.- Variation with lift coefficient of the aerodynamic characteristics of the basic configuration with pylon-suspended nacelles N.

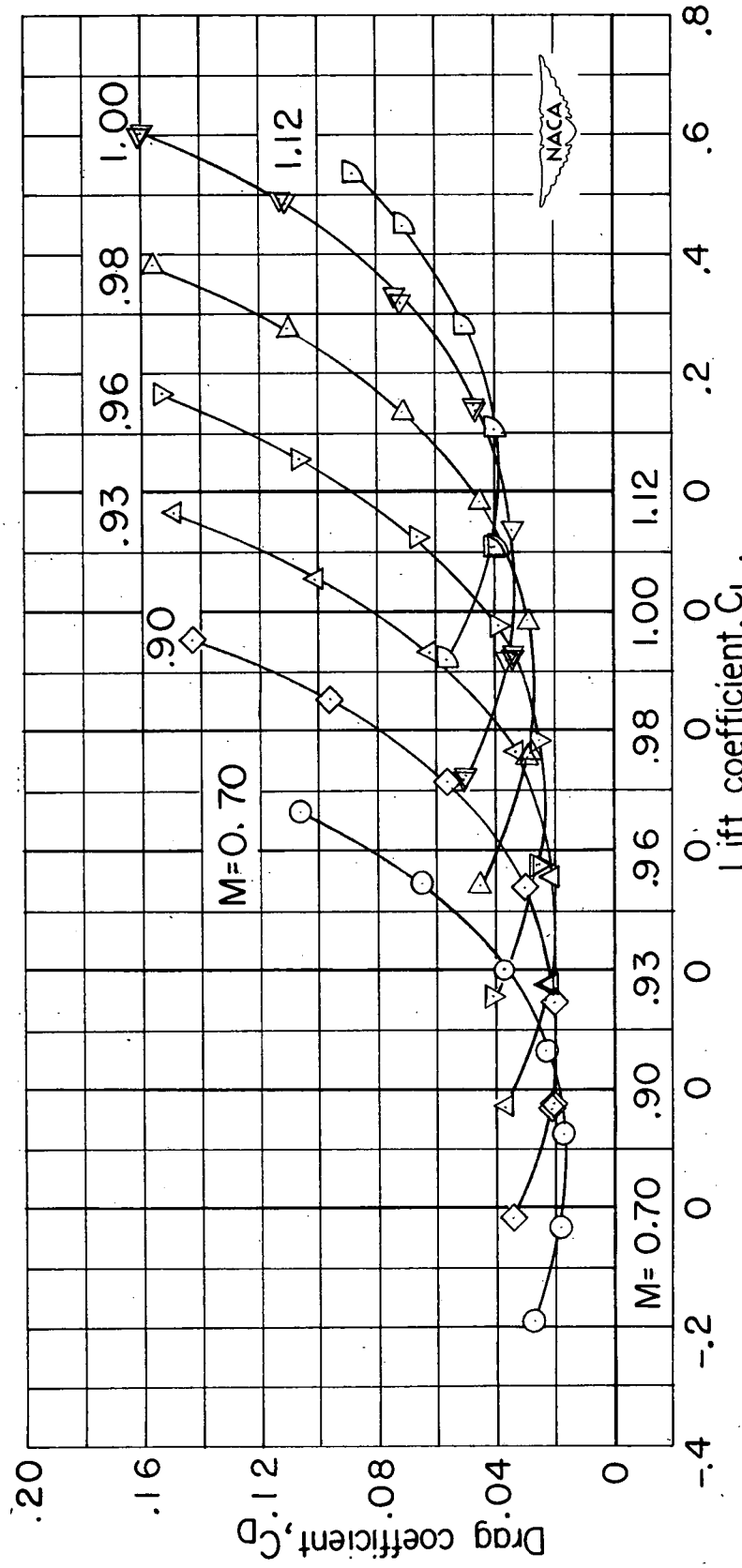

(b) Drag coefficient.

Figure 8.- Continued.

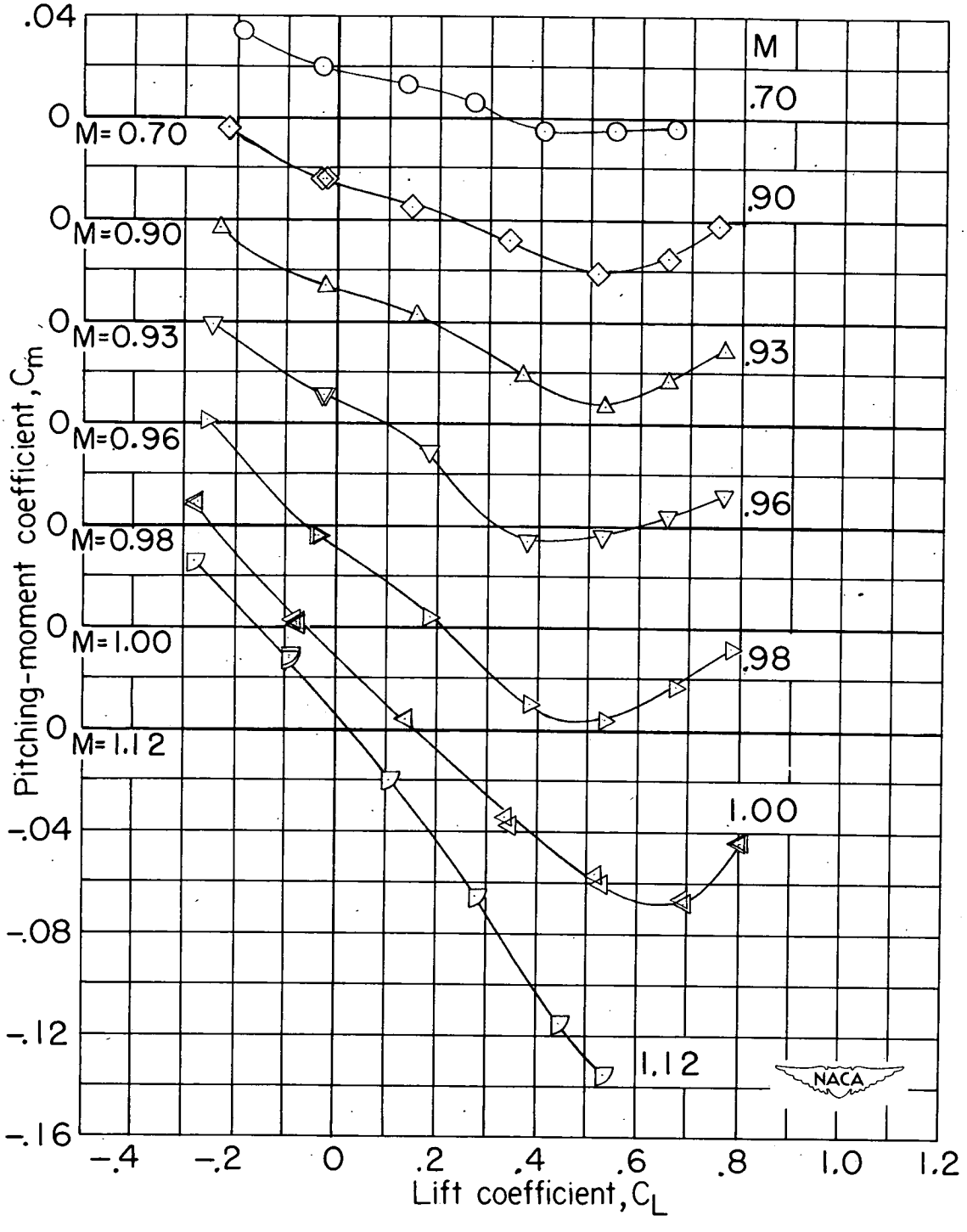

(c) Pitching-moment coefficient.

Figure 8.- Concluded.

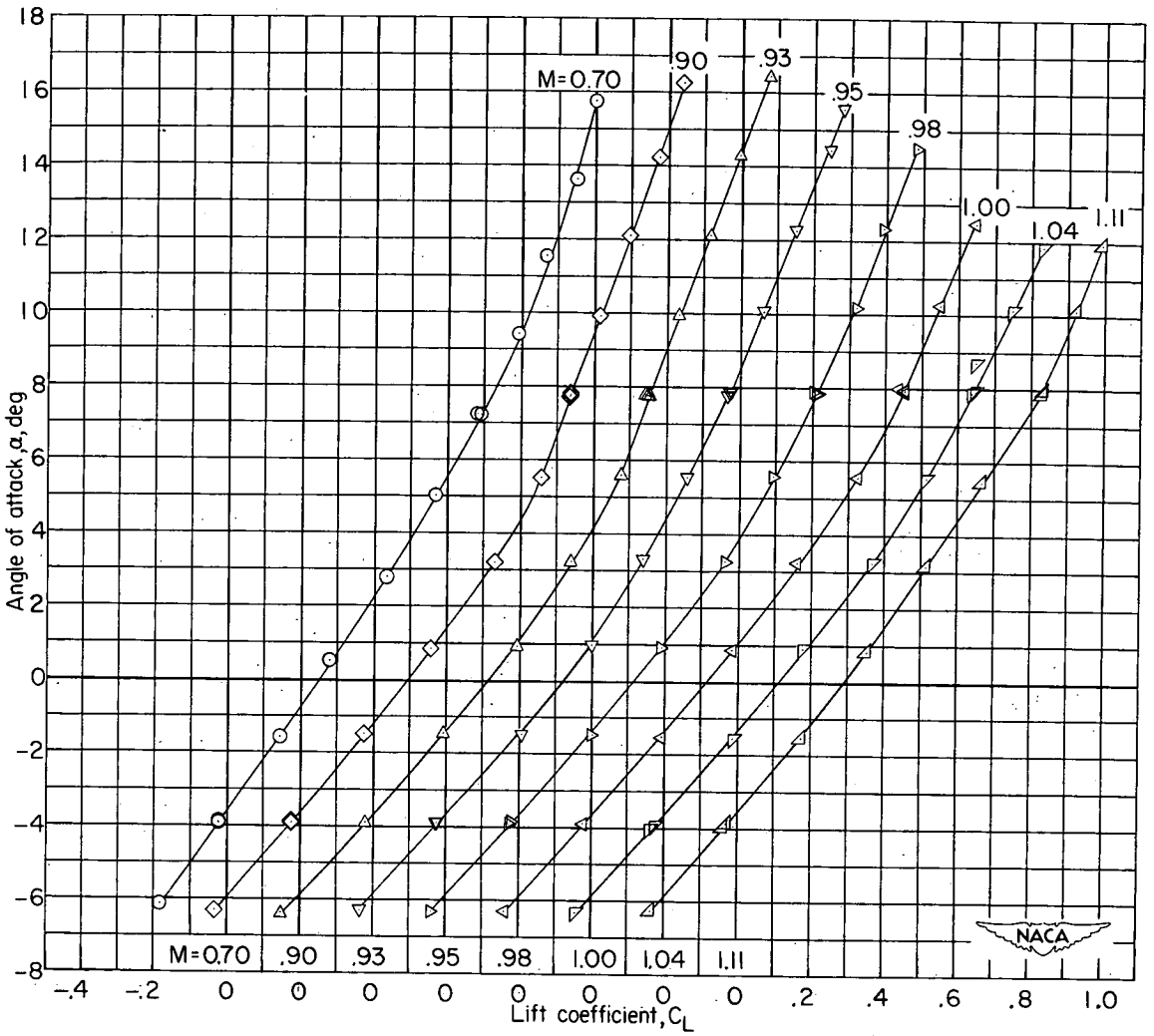

(a) Angle of attack.

Figure 9.- Variation with lift coefficient of the aerodynamic characteristics of the basic configuration with buried nacelles N_2.

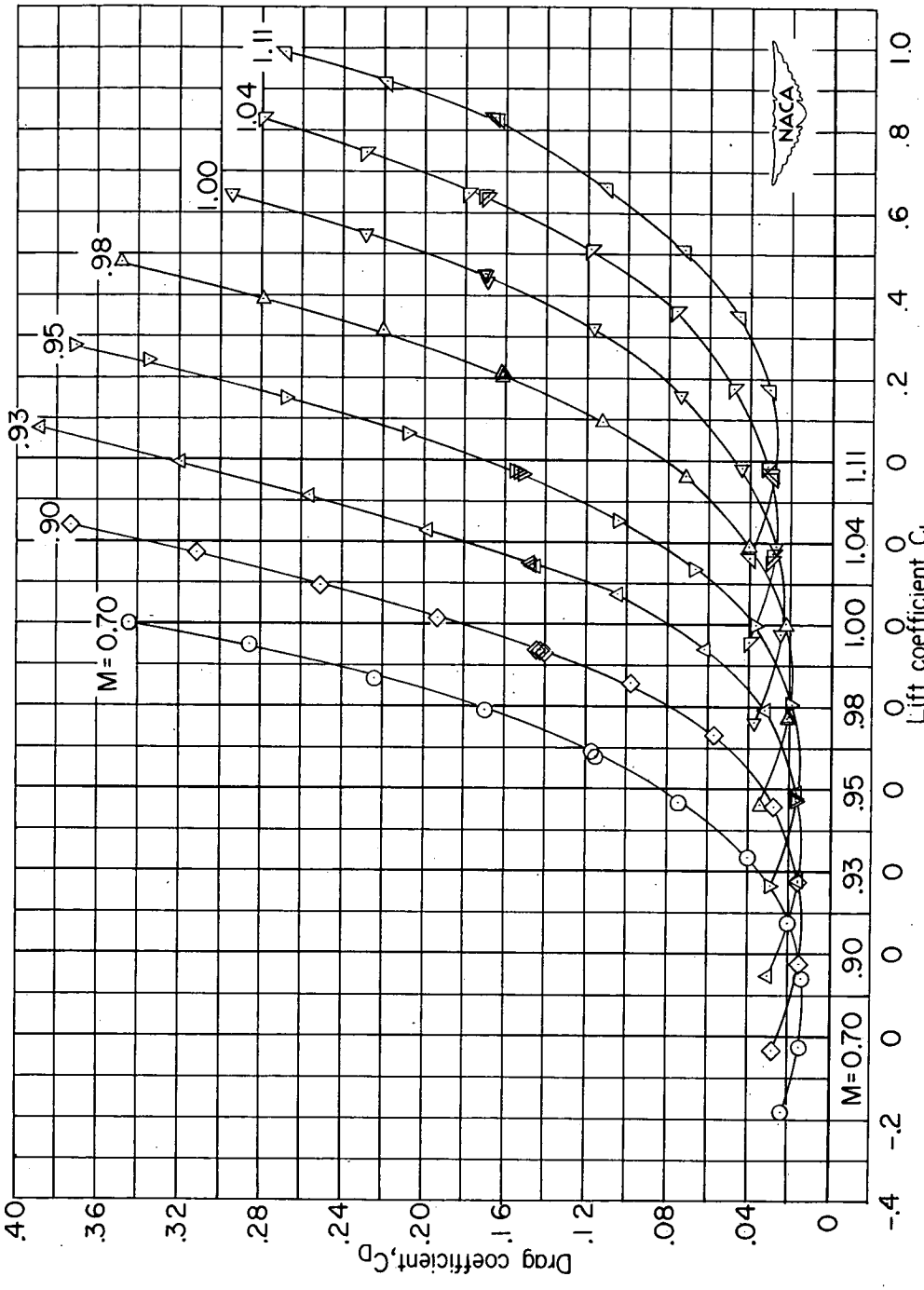

(b) Drag coefficient.

Figure 9.- Continued.

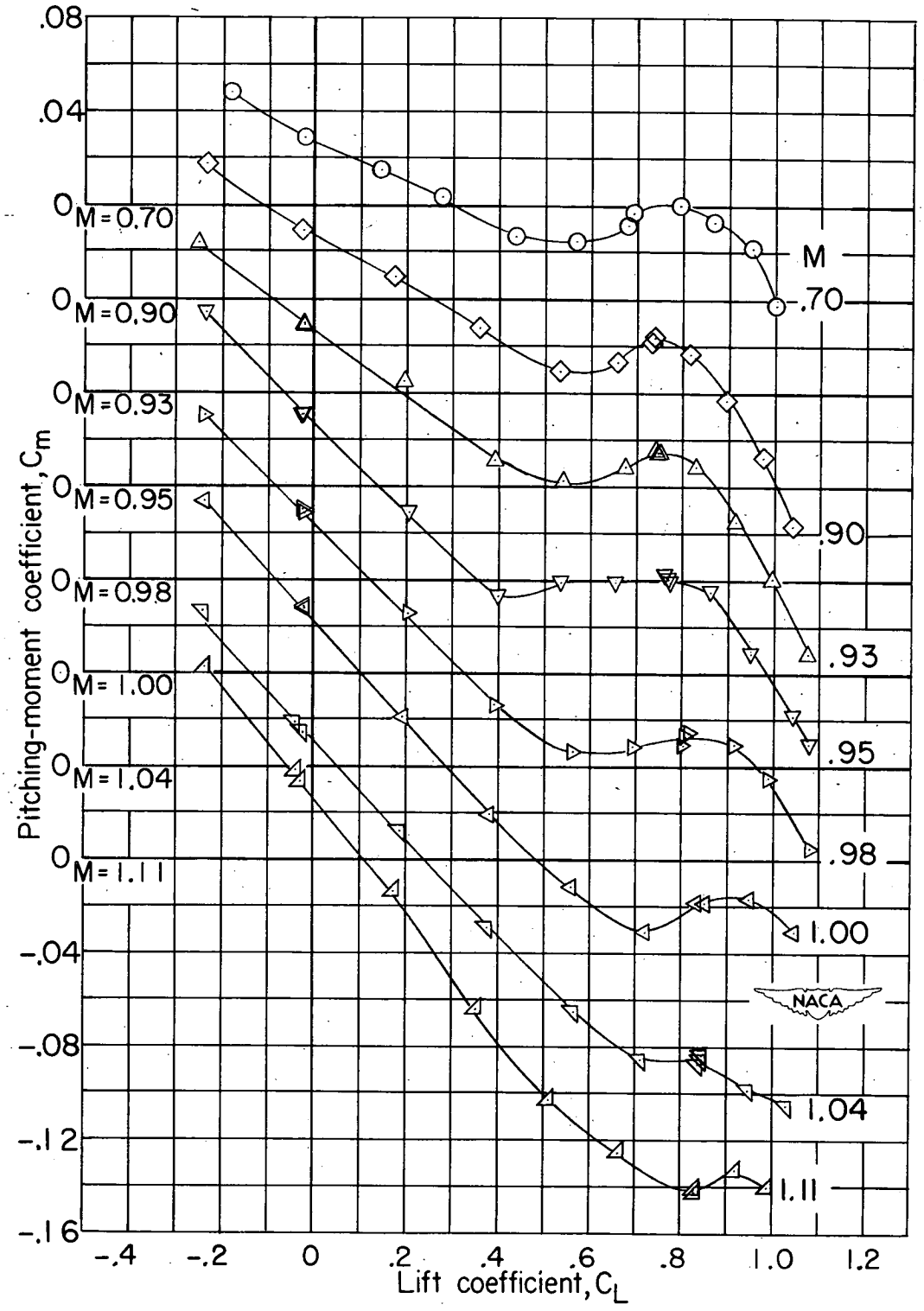

(c) Pitching-moment coefficient.

Figure 9.- Concluded.

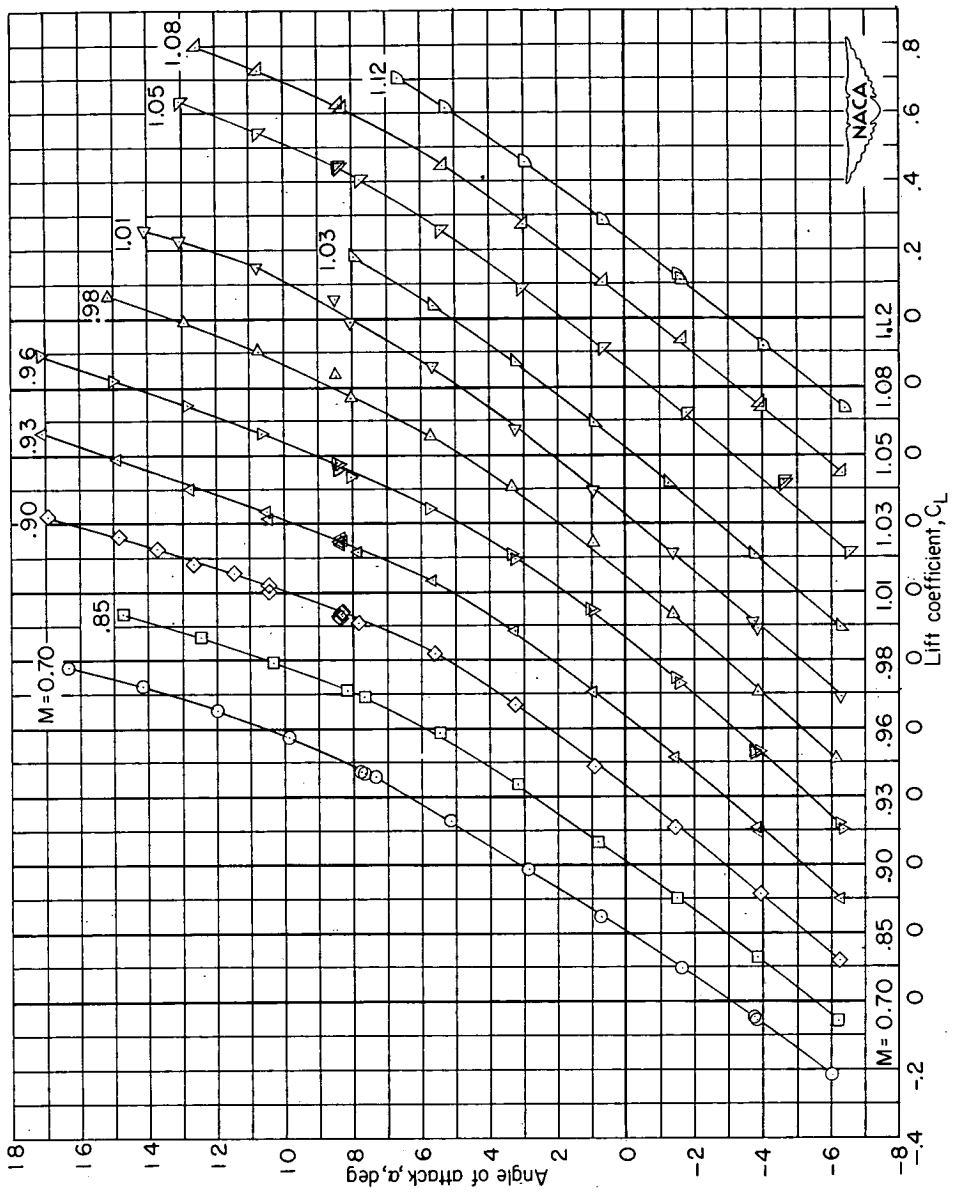

(a) Angle of attack.

Figure 10.- Variation with lift coefficient of the aerodynamic characteristics of the basic configuration with pylon-suspended nacelles N3.

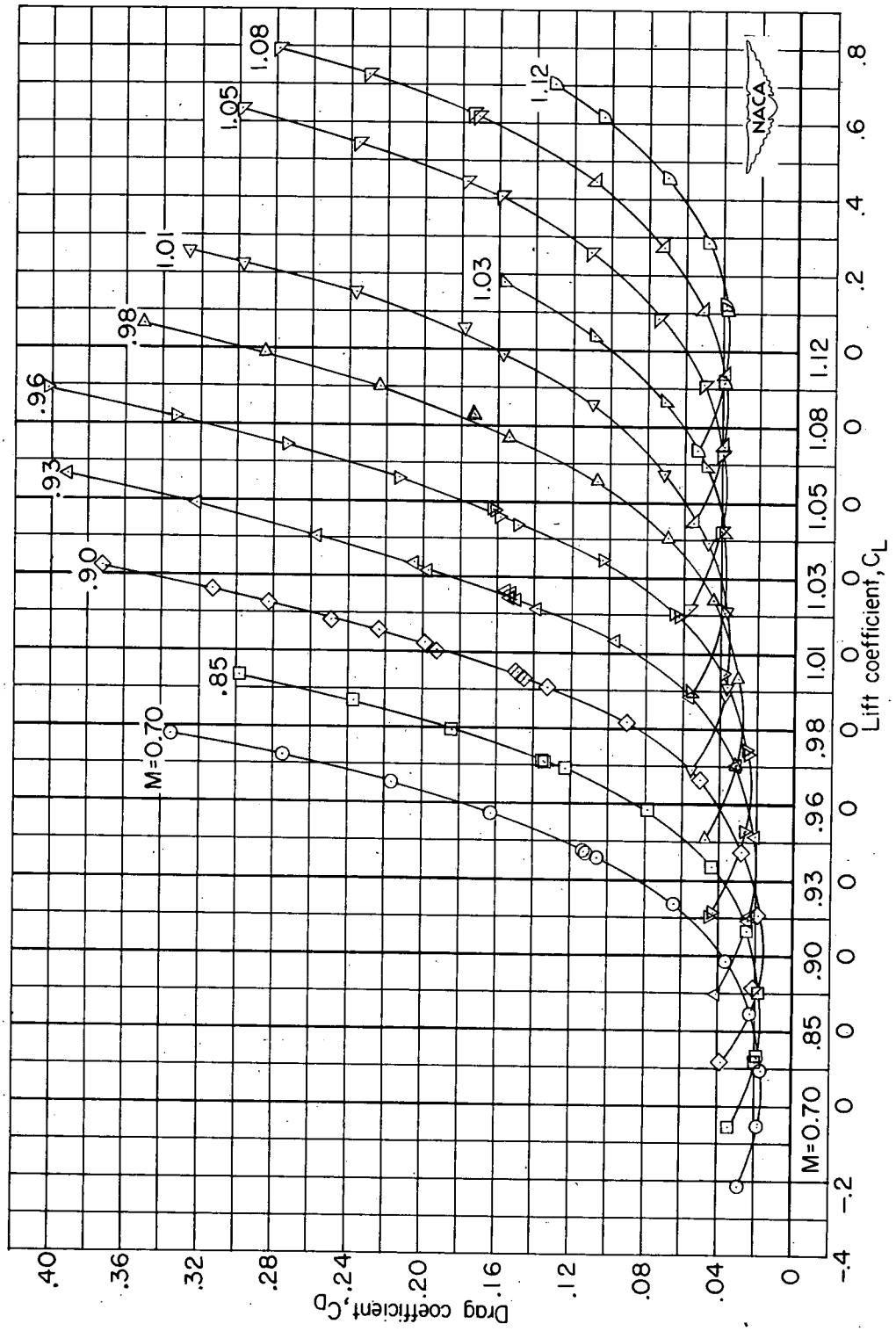

(b) Drag coefficient.

Figure 10.- Continued.

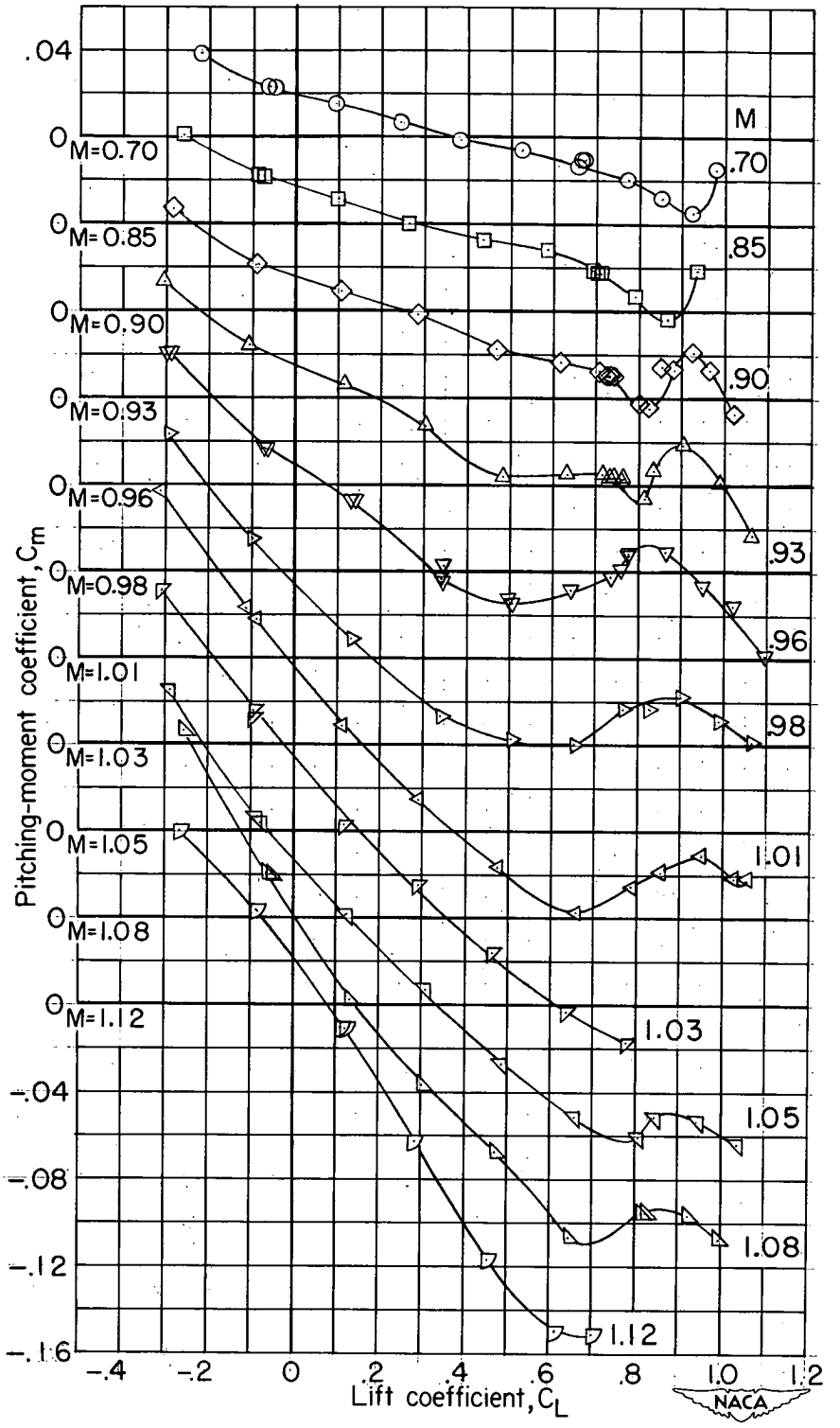

(c) Pitching-moment coefficient.

Figure 10.- Concluded.

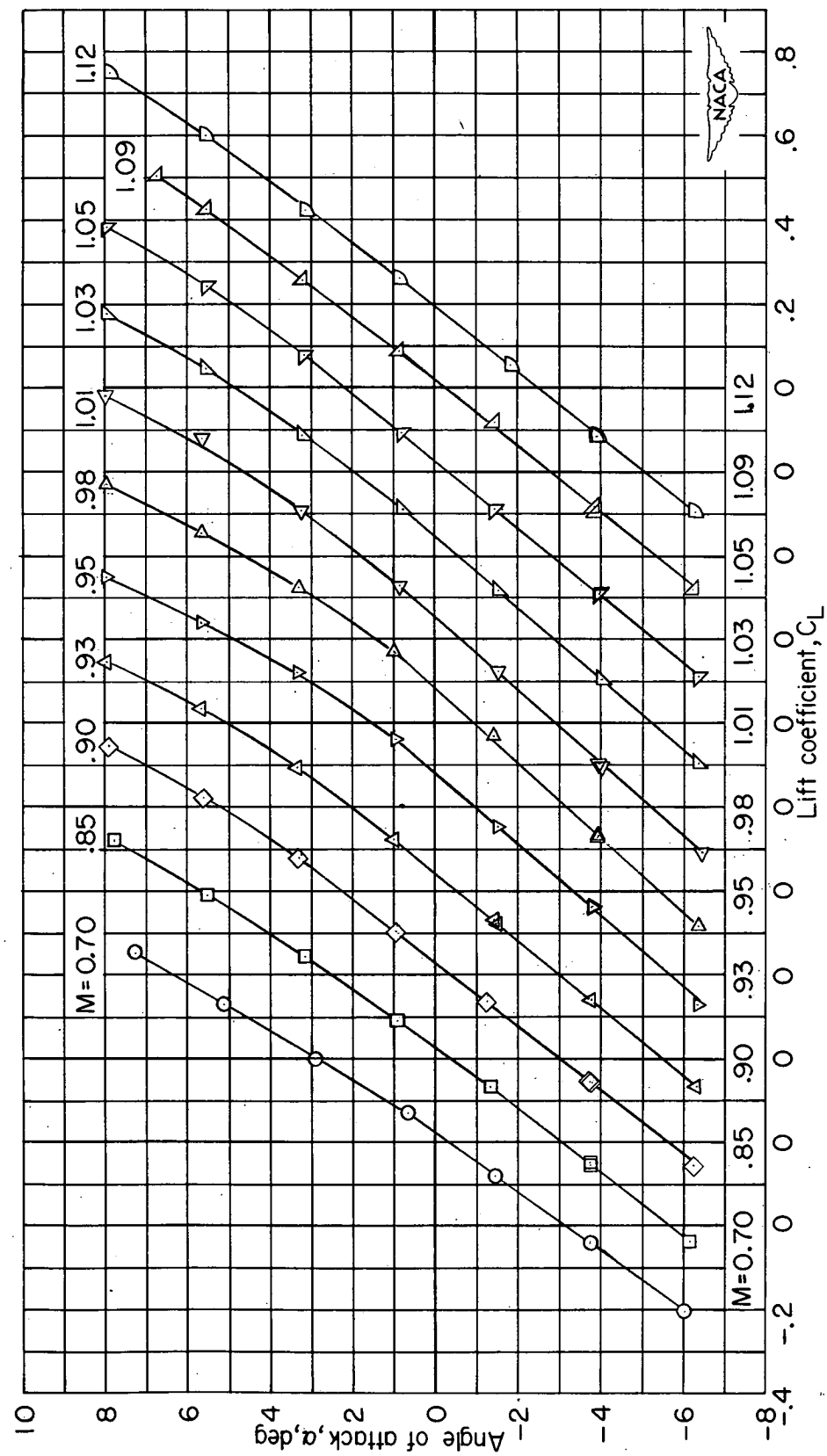

(a) Angle of attack.

Figure 11.- Variation with lift coefficient of the aerodynamic characteristics of the basic configuration with pylon-suspended nacelles N_4.

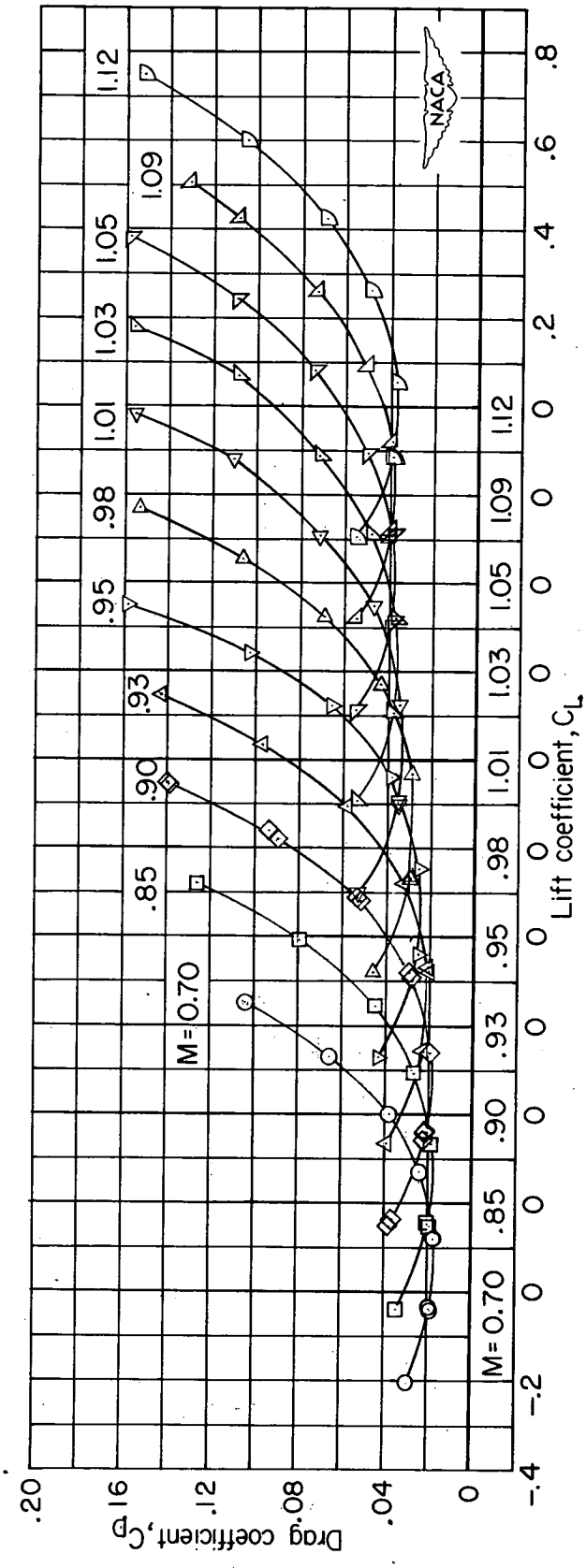

(b) Drag coefficient.

Figure 11.- Continued.

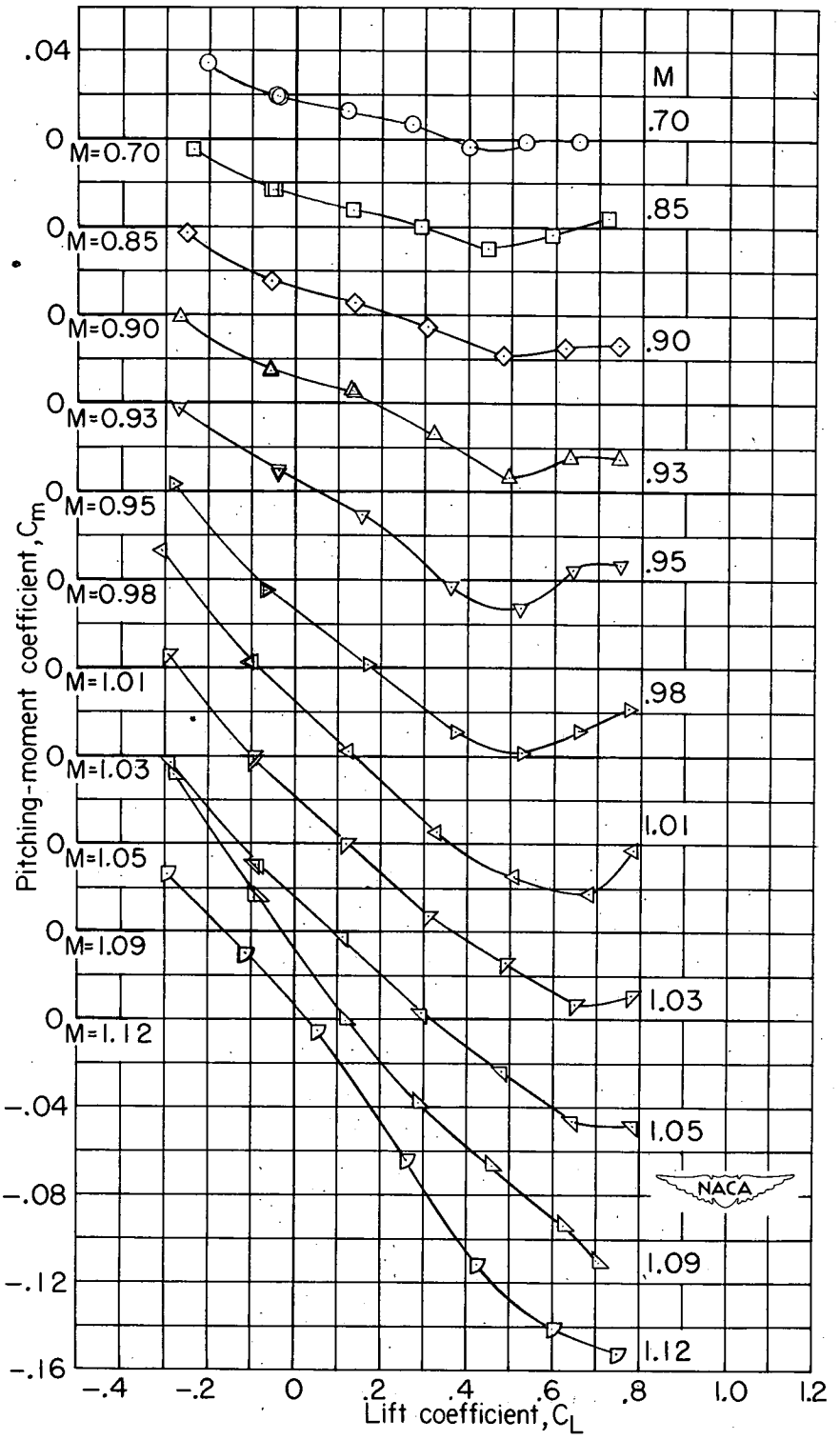

(c) Pitching-moment coefficient.

Figure 11.- Concluded.

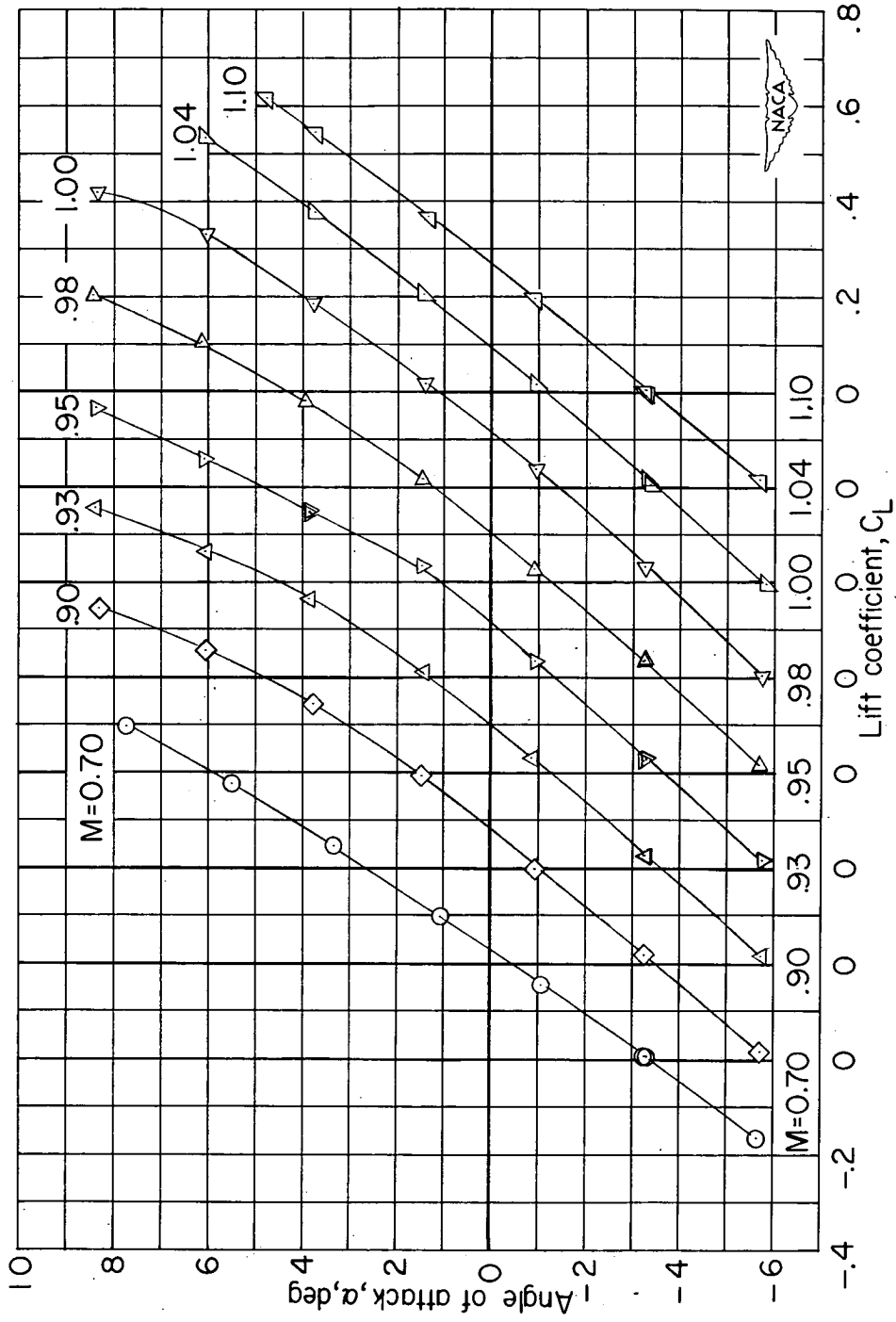

(a) Angle of attack.

Figure 12.- Variation with lift coefficient of the aerodynamic characteristics of the basic configuration with underslung nacelles N_5.

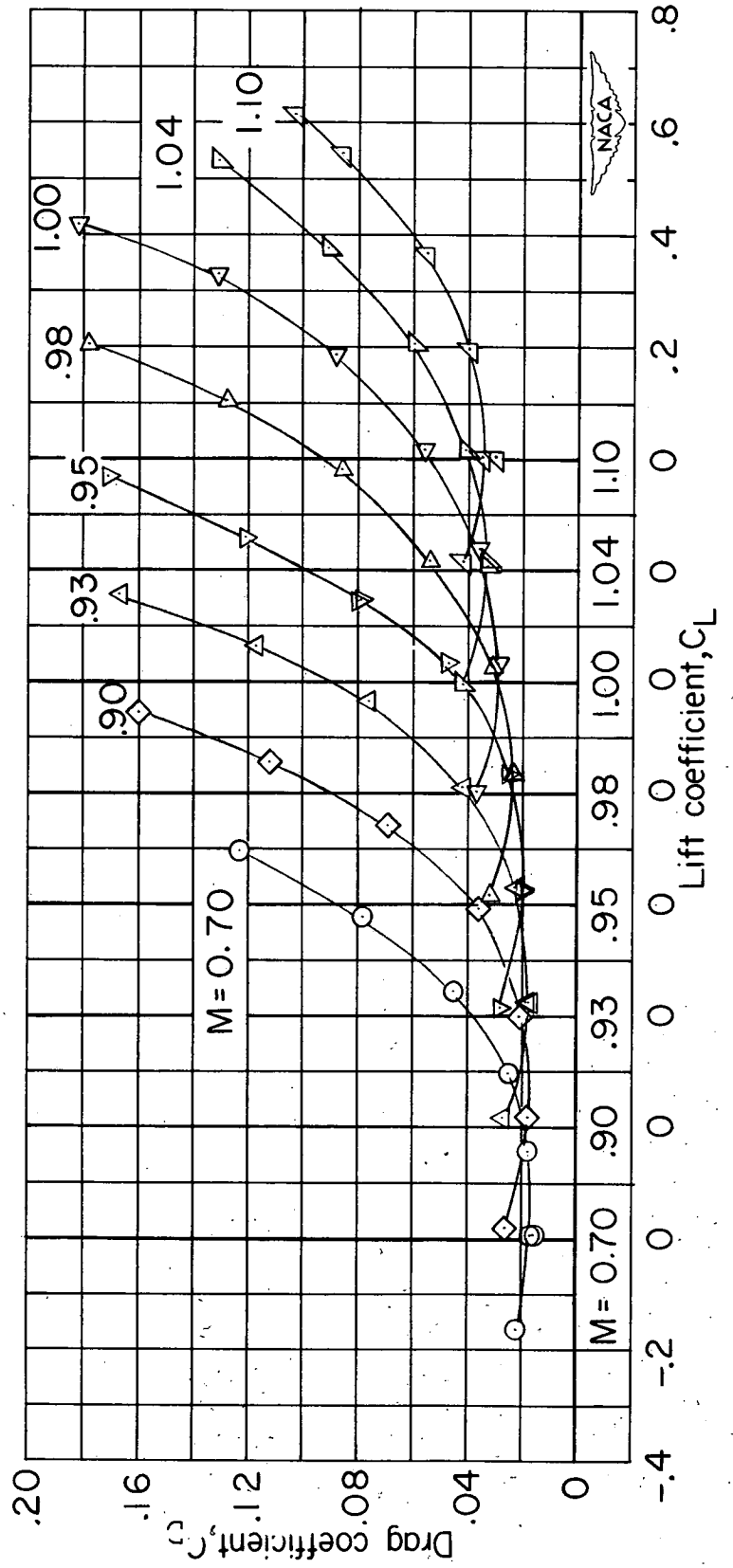

(b) Drag coefficient.

Figure 12.- Continued.

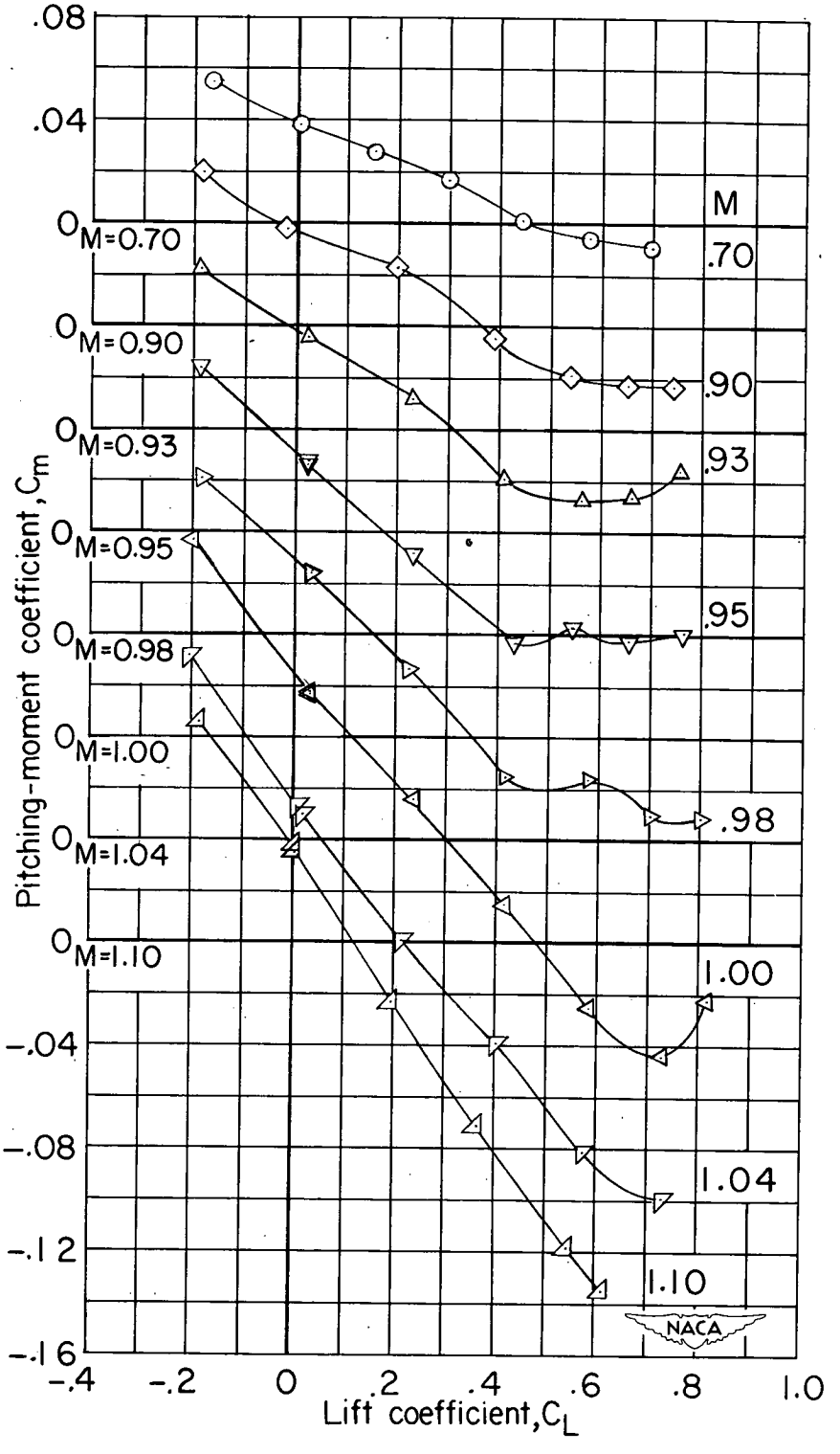

(c) Pitching-moment coefficient.

Figure 12.- Concluded.

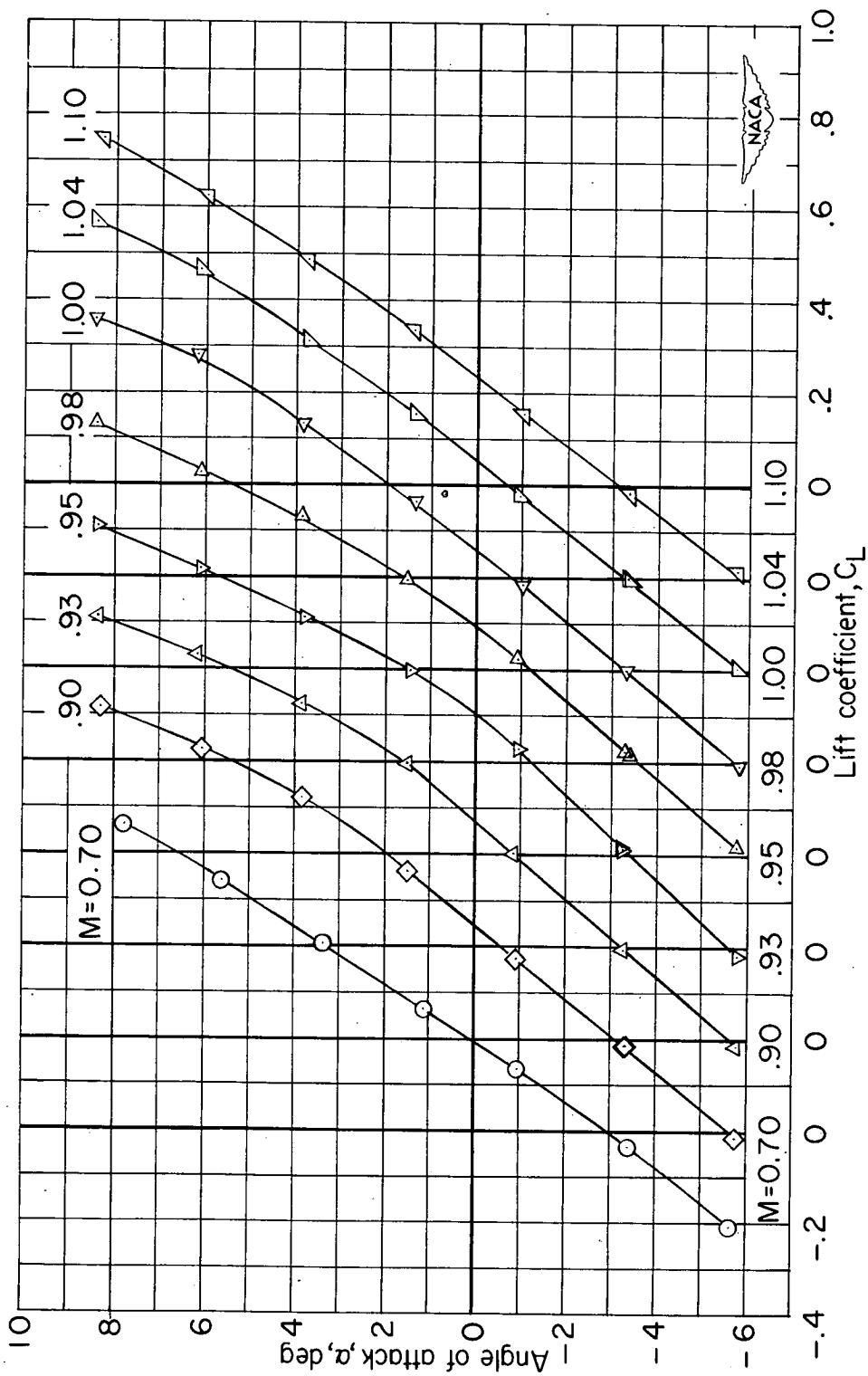

(a) Angle of attack.

Figure 13.- Variation with lift coefficient of the aerodynamic characteristics of the basic configuration with underslung nacelles N6.

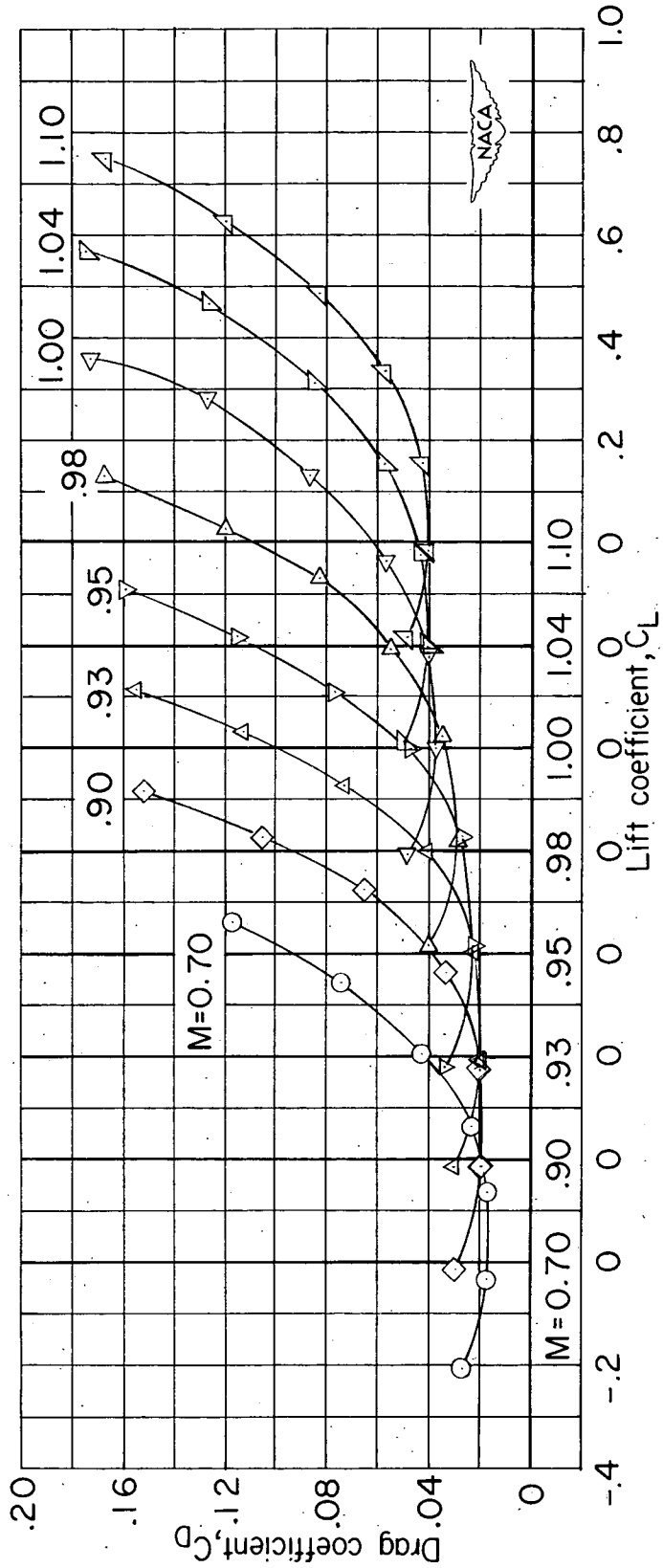

(b) Drag coefficient.

Figure 13.- Continued.

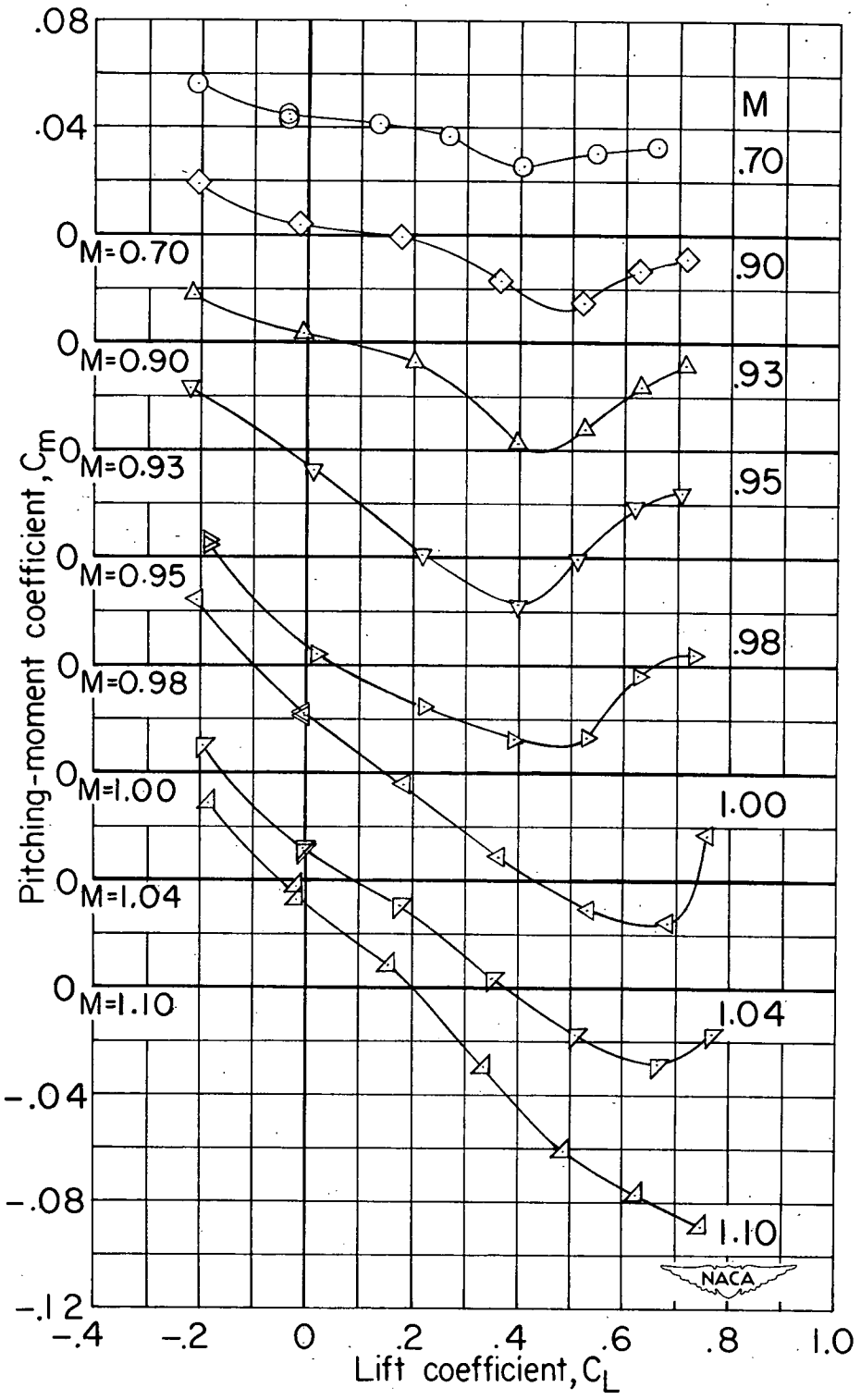

(c) Pitching-moment coefficient.

Figure 13.- Concluded.

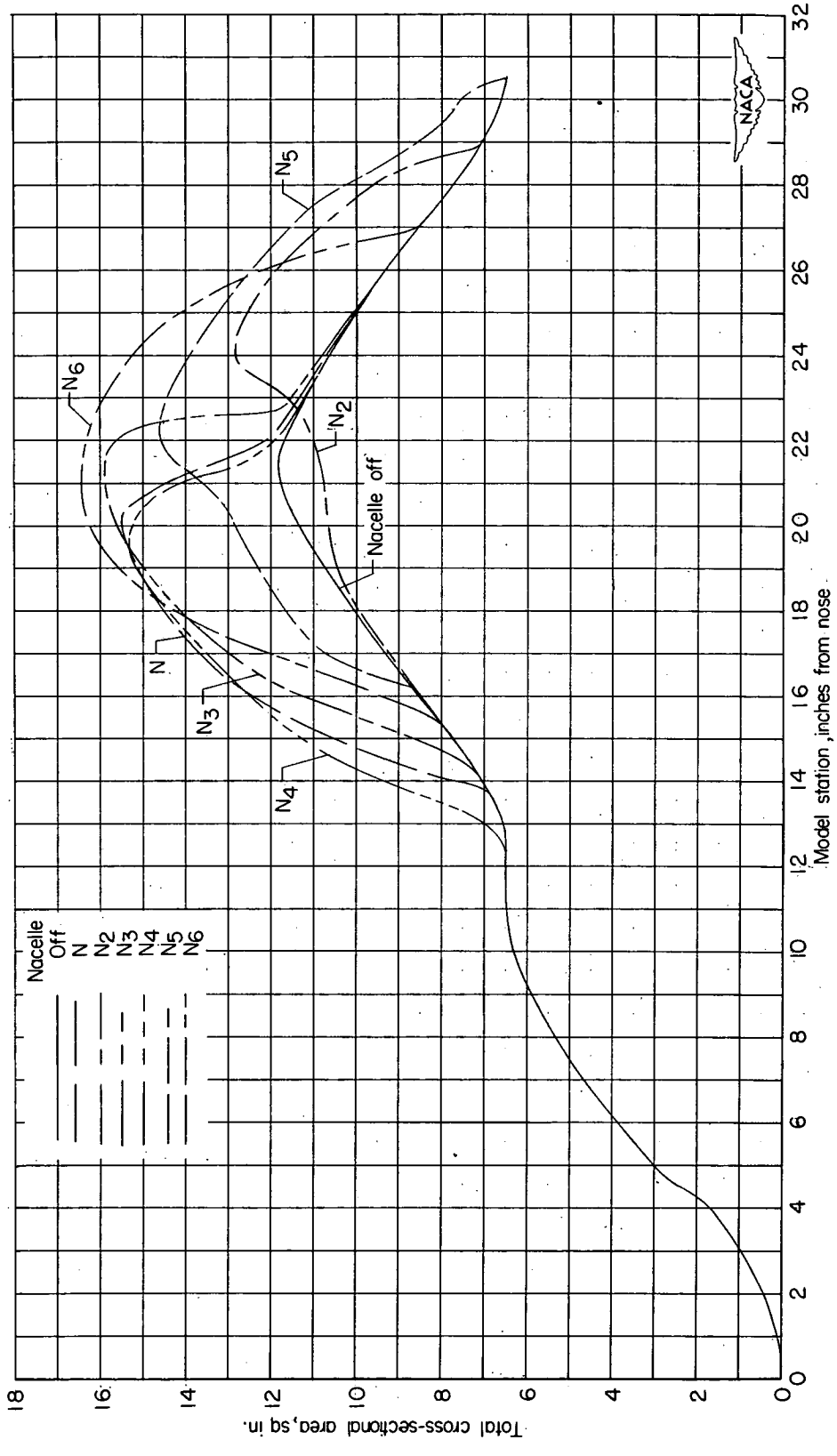

Figure 14.- The axial distribution of total cross-sectional area for the various configurations.

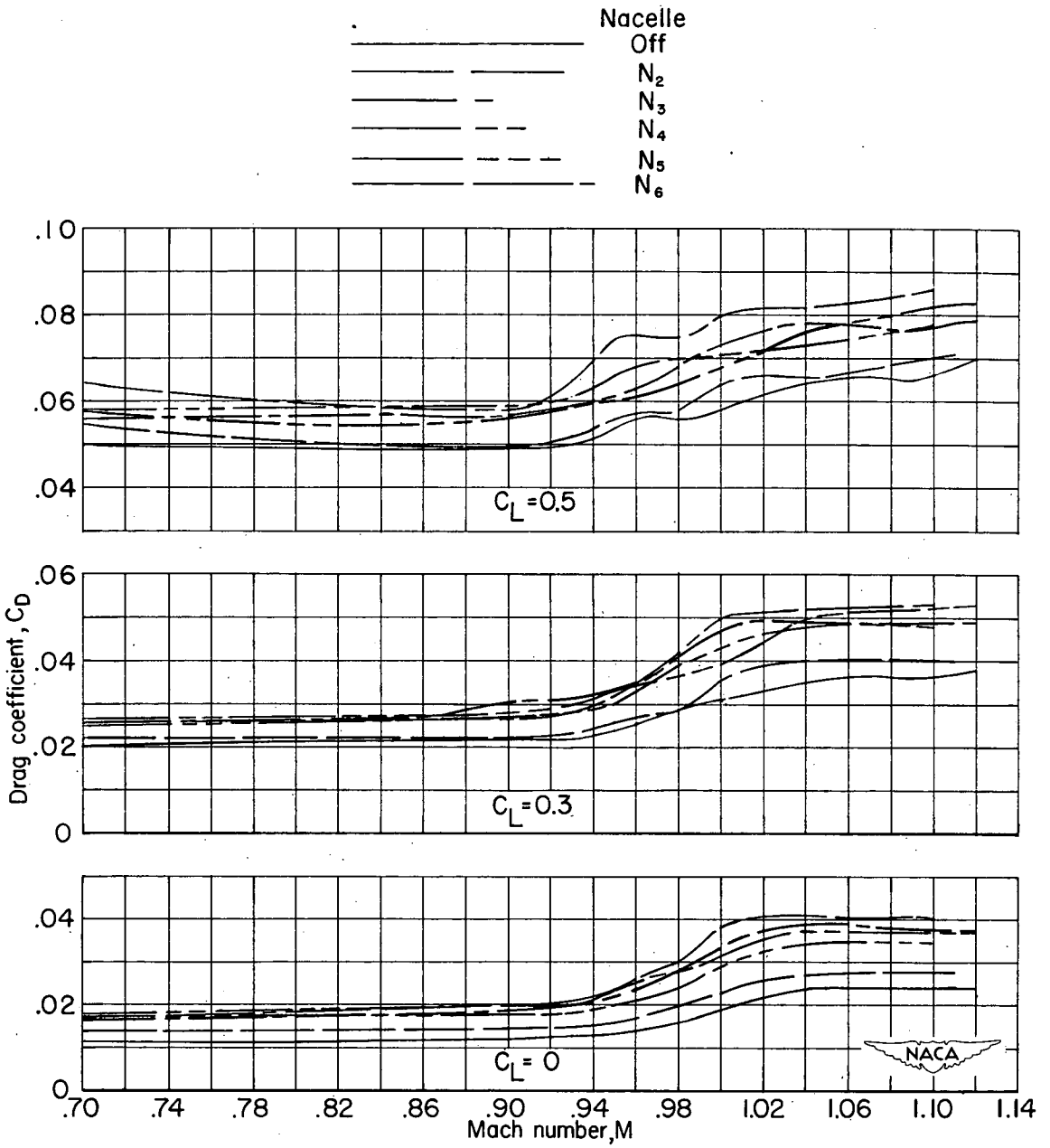

Figure 15.- A comparison of the drag characteristics of the various configurations.

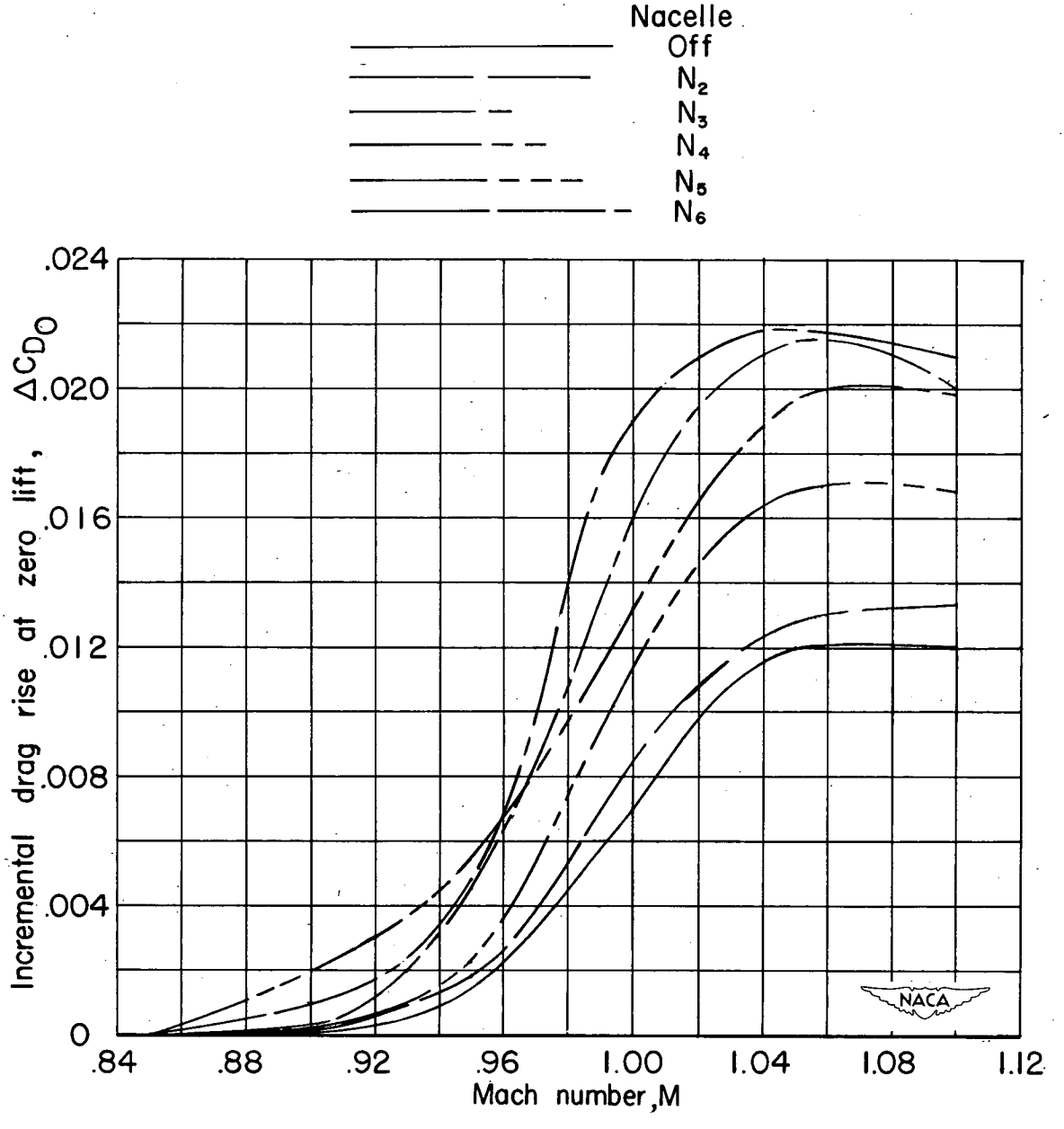

Figure 16.- A comparison of the incremental drag-rise characteristics at zero lift of the various configurations.

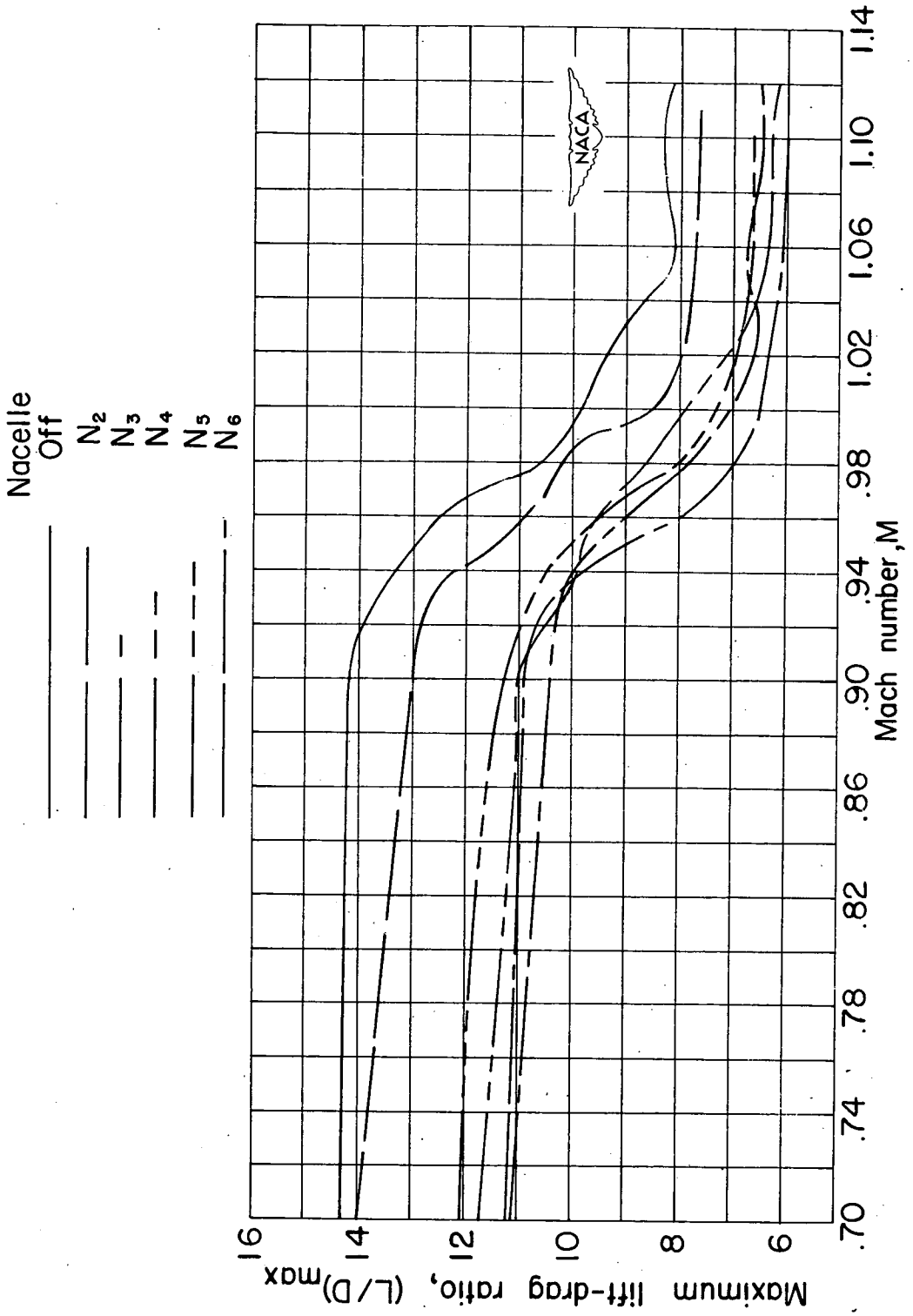

Figure 17.- A comparison of the maximum lift-drag ratios of the various configurations.

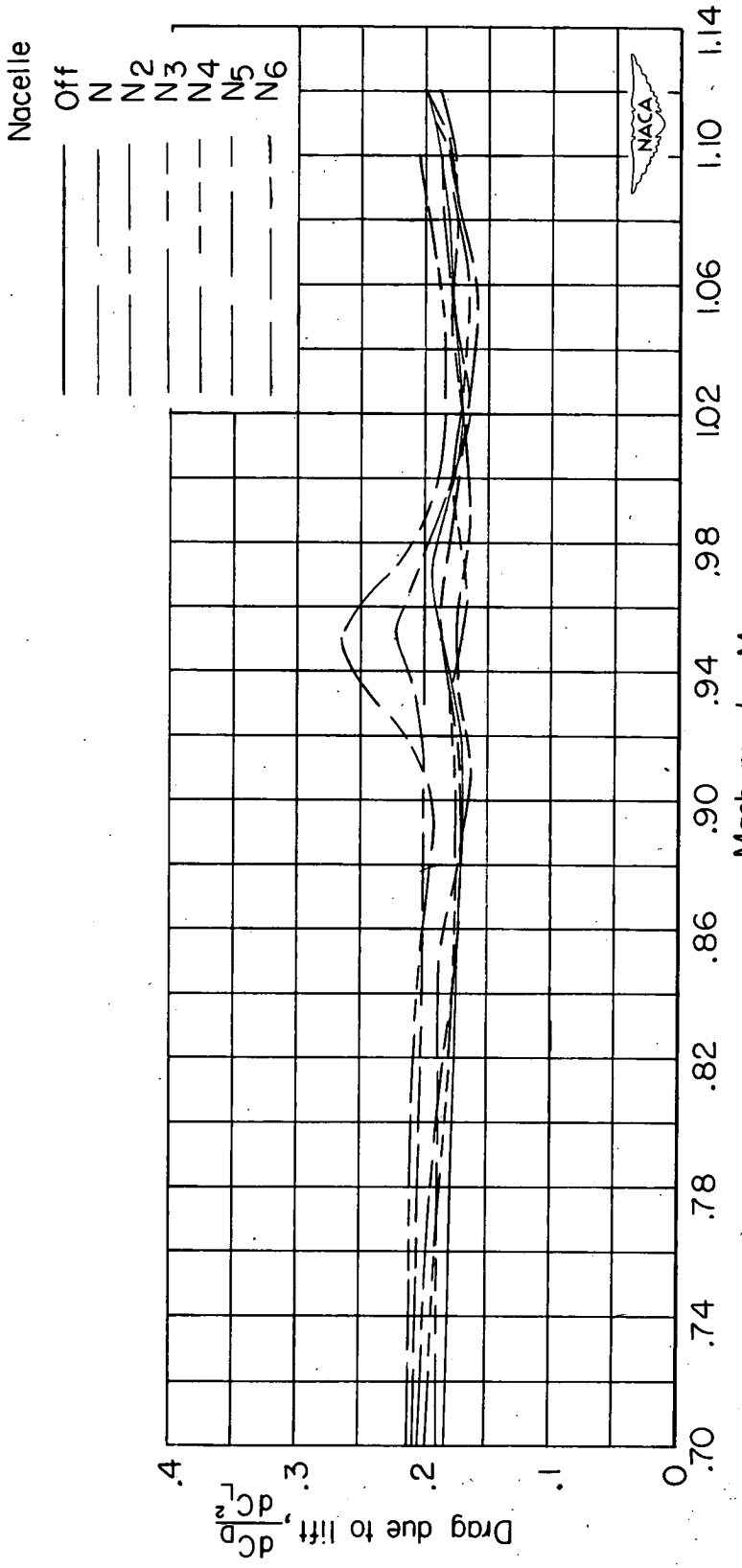

Figure 18.- A comparison of drag due to lift of the various configurations.

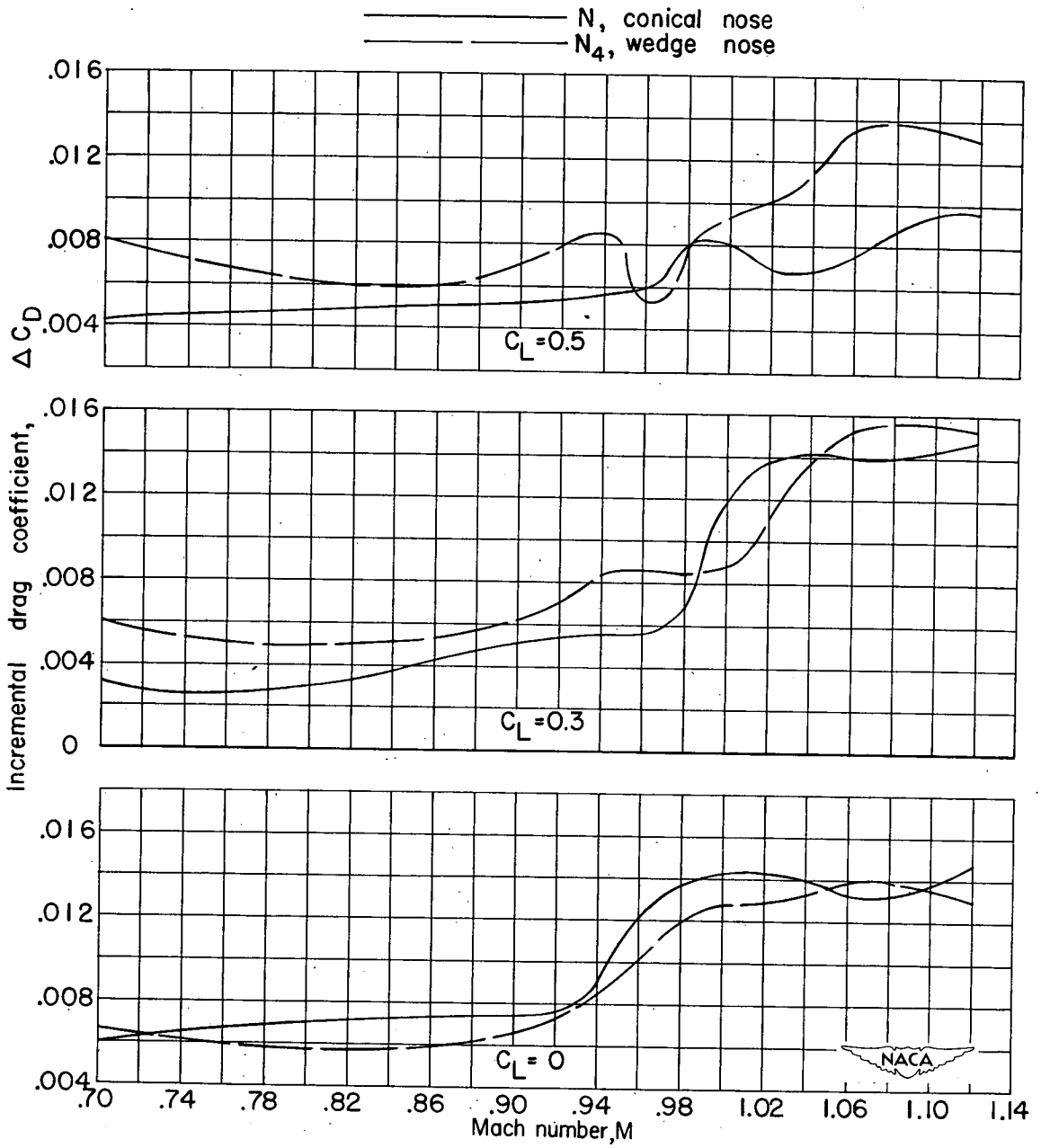

Figure 19.- Effect of nacelle nose shape on the incremental drag coefficients of the pylon-suspended nacelles.

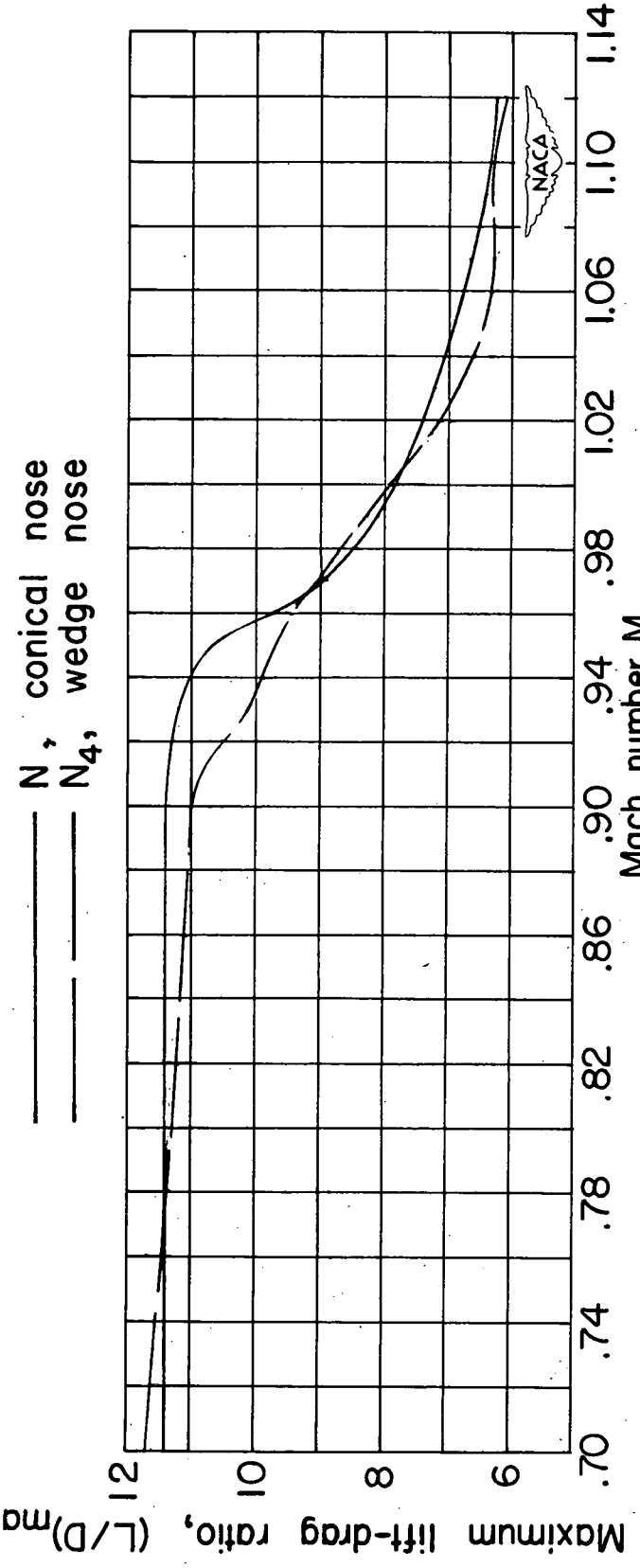

Figure 20.- Effect of nacelle nose shape on the maximum lift-drag ratios of the pylon-suspended nacelles.

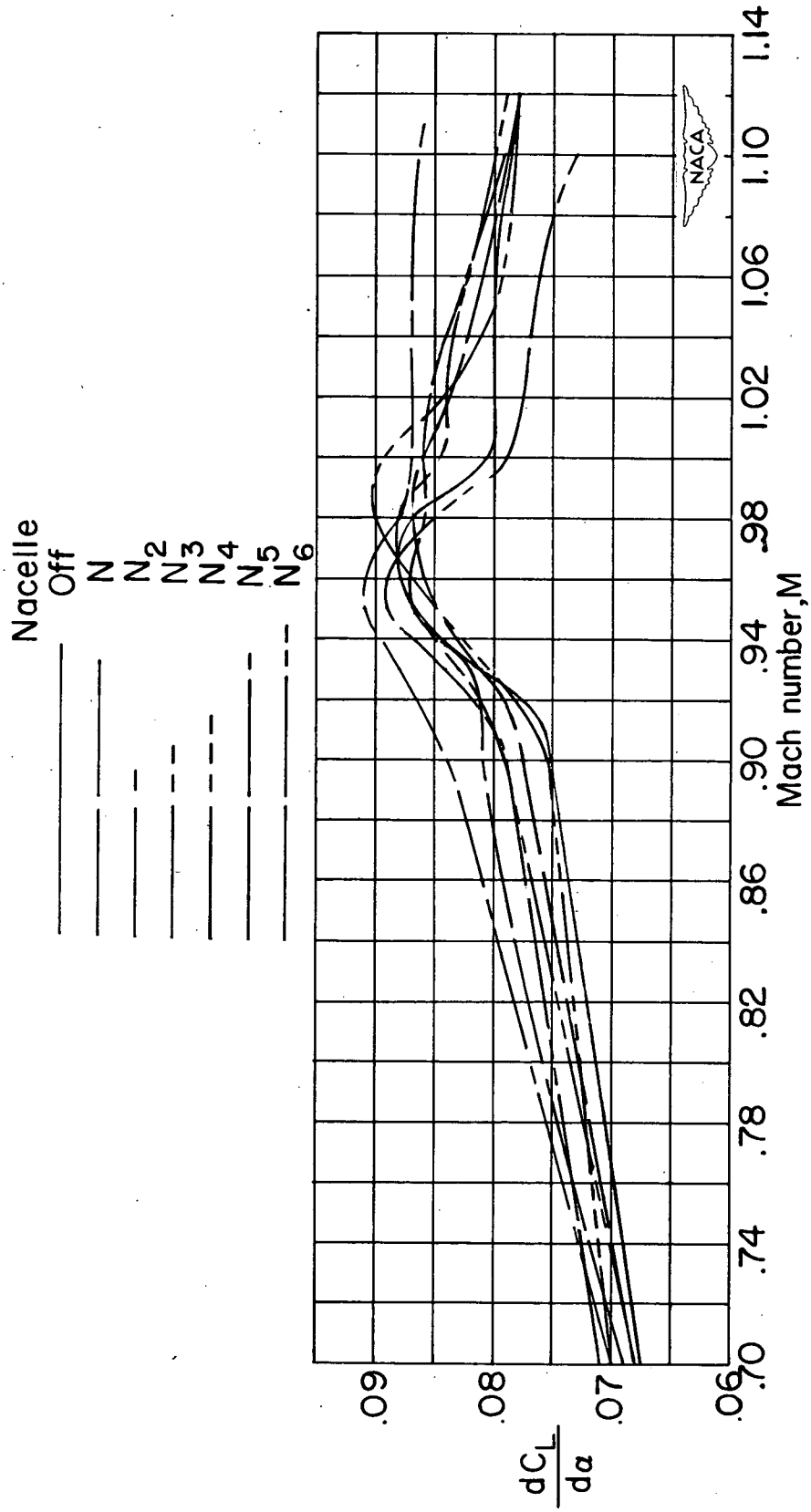

Figure 21.- A comparison of the lift-curve slopes of the various configurations.

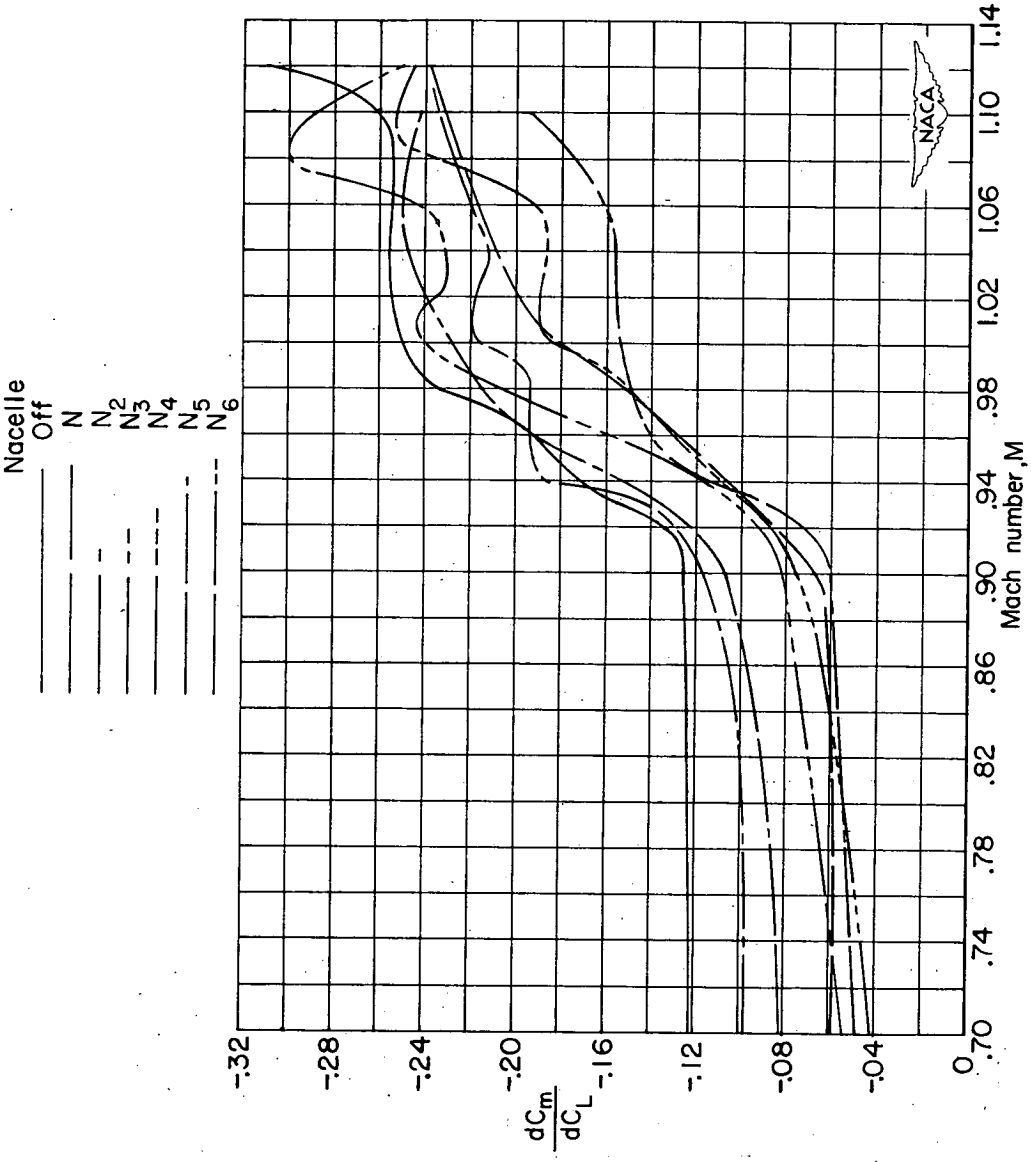

Figure 22.- A comparison of the pitching-moment-curve slopes of the various configurations.

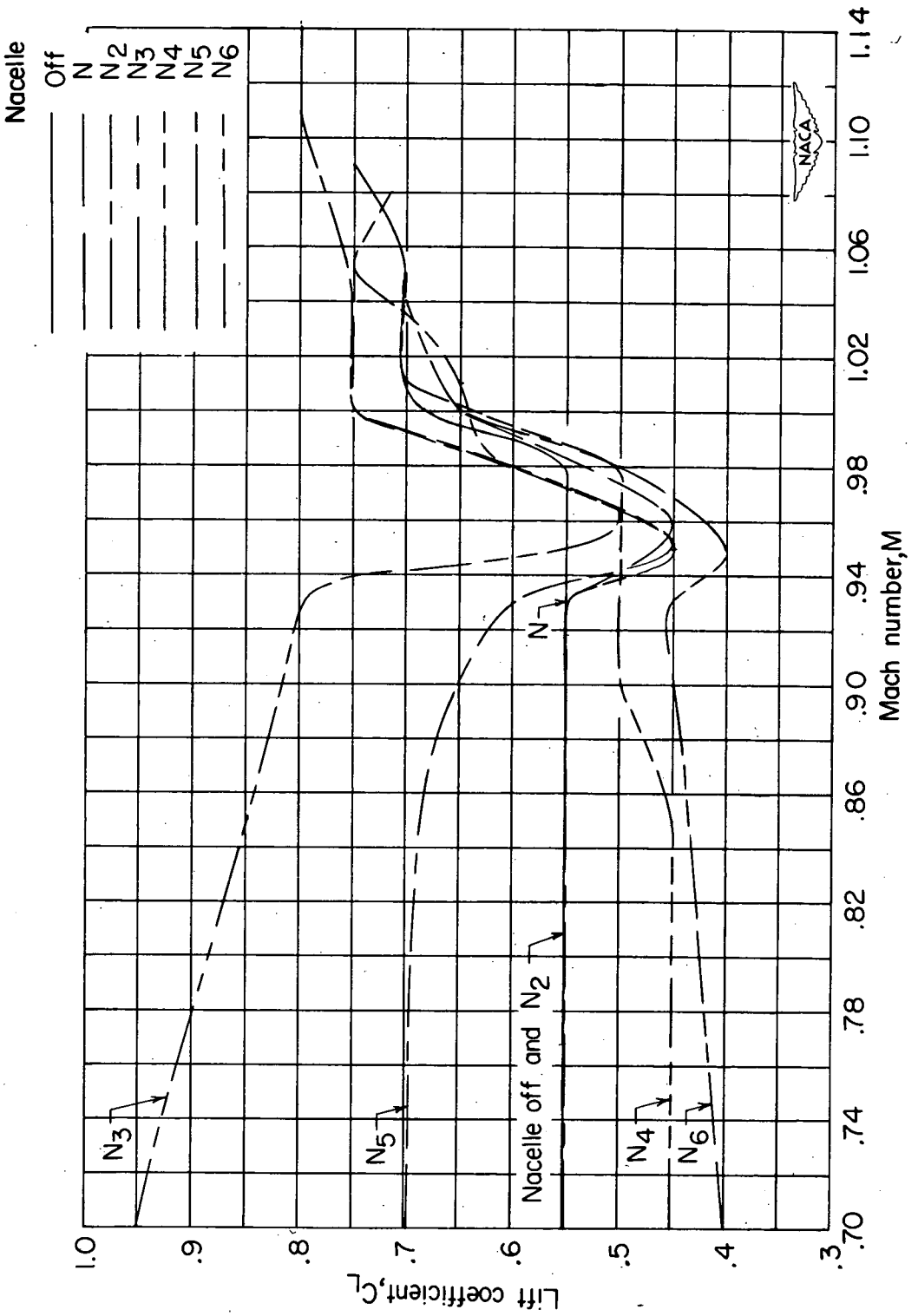

Figure 23.- A comparison of the lift coefficient at pitch-up for the various configurations.

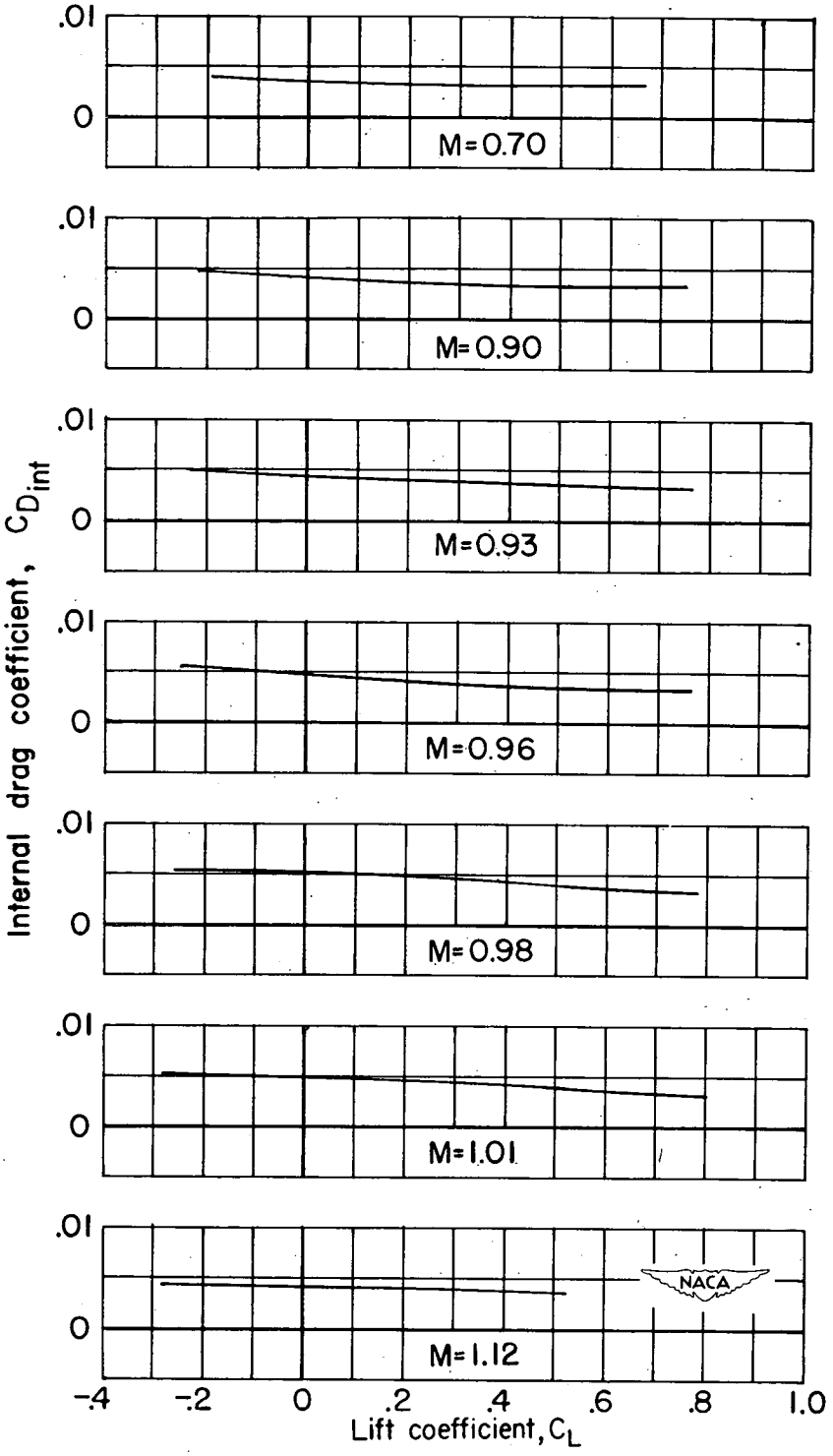

(a) Pylon-suspended nacelles N.

Figure 24.- The internal-drag coefficients for several of the nacelles.

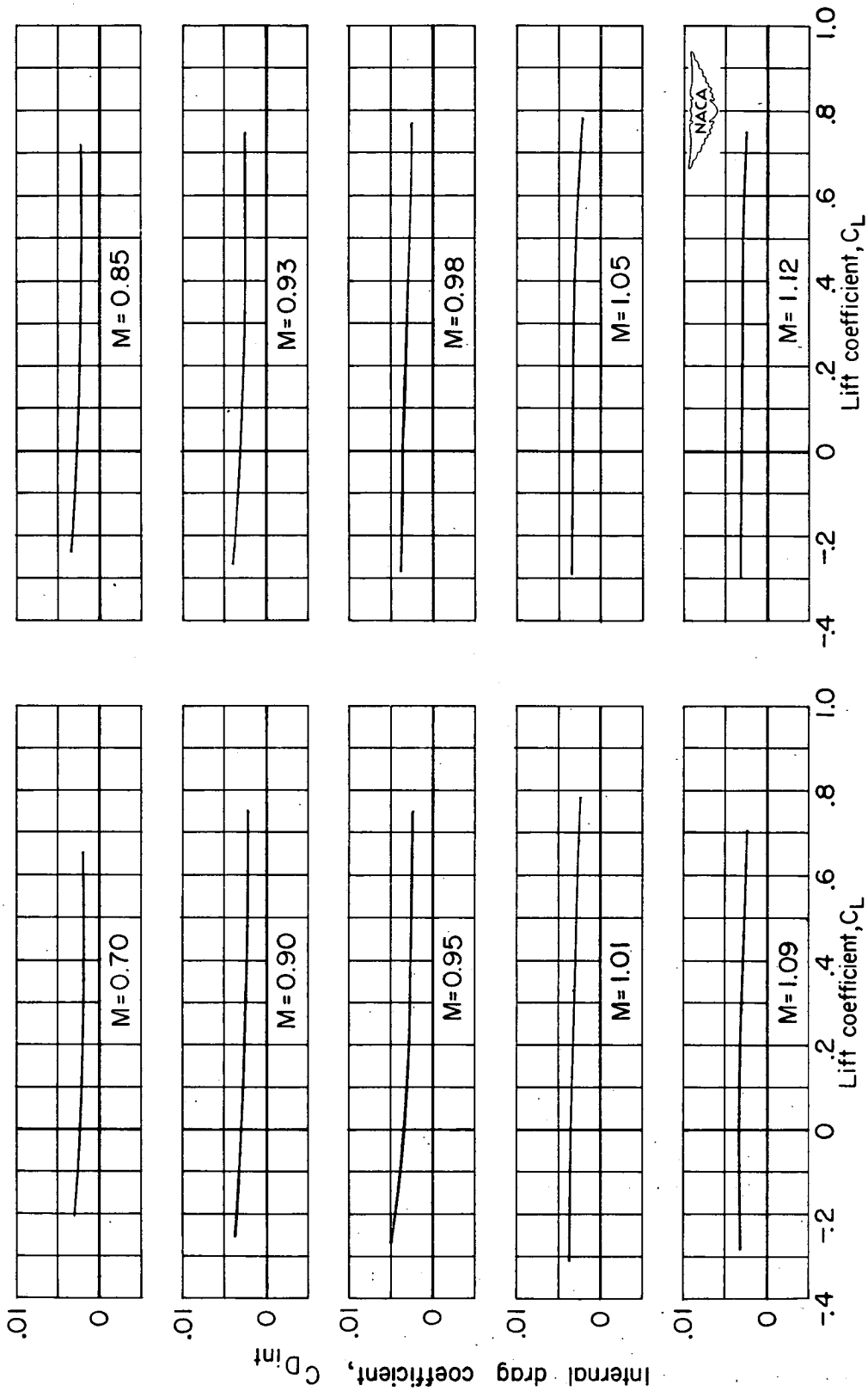

(b) Pylon-suspended nacelles N_4.

Figure 24.- Continued.

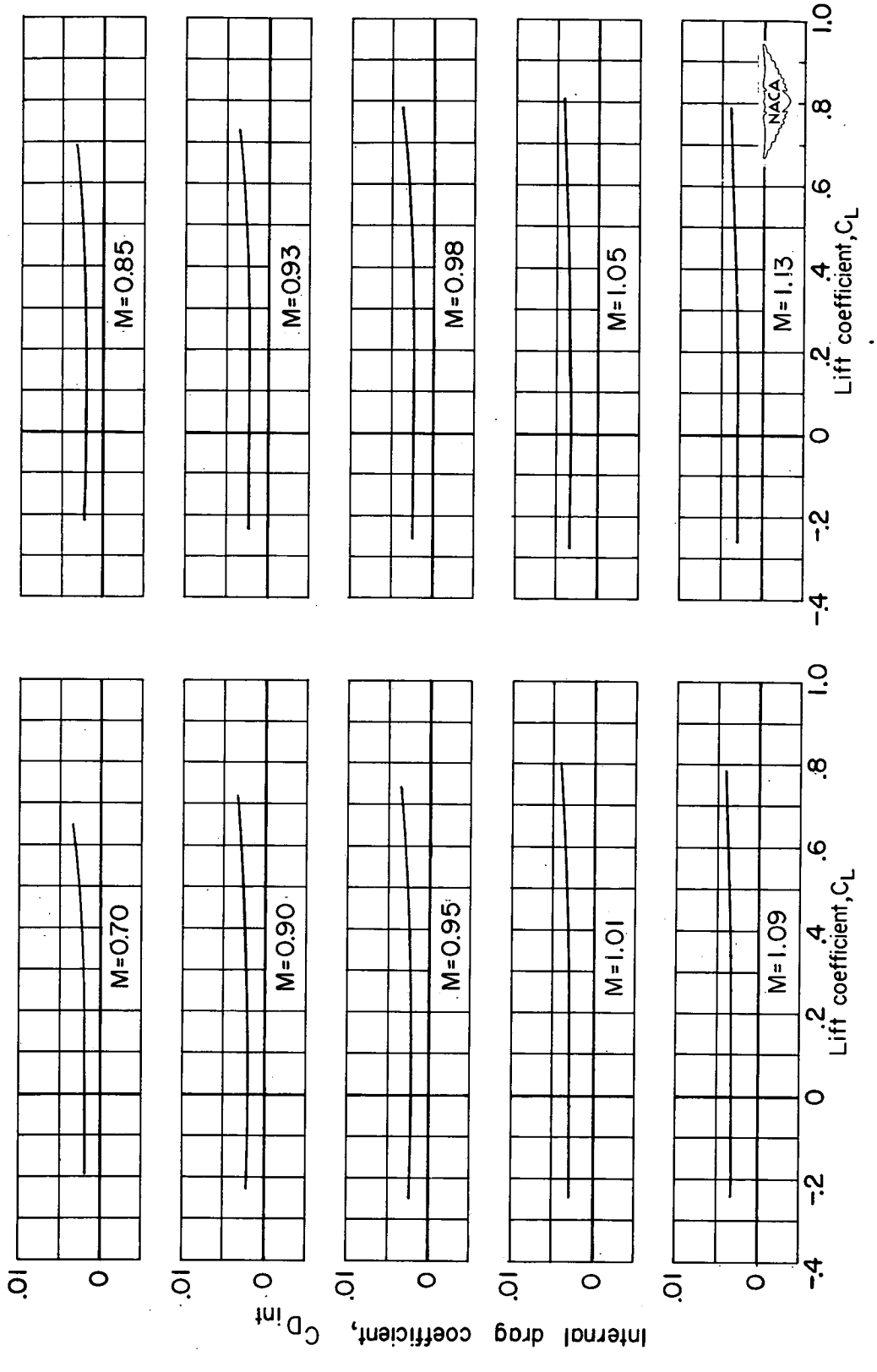

(c) Buried nacelles N_2.

Figure 24.- Concluded.

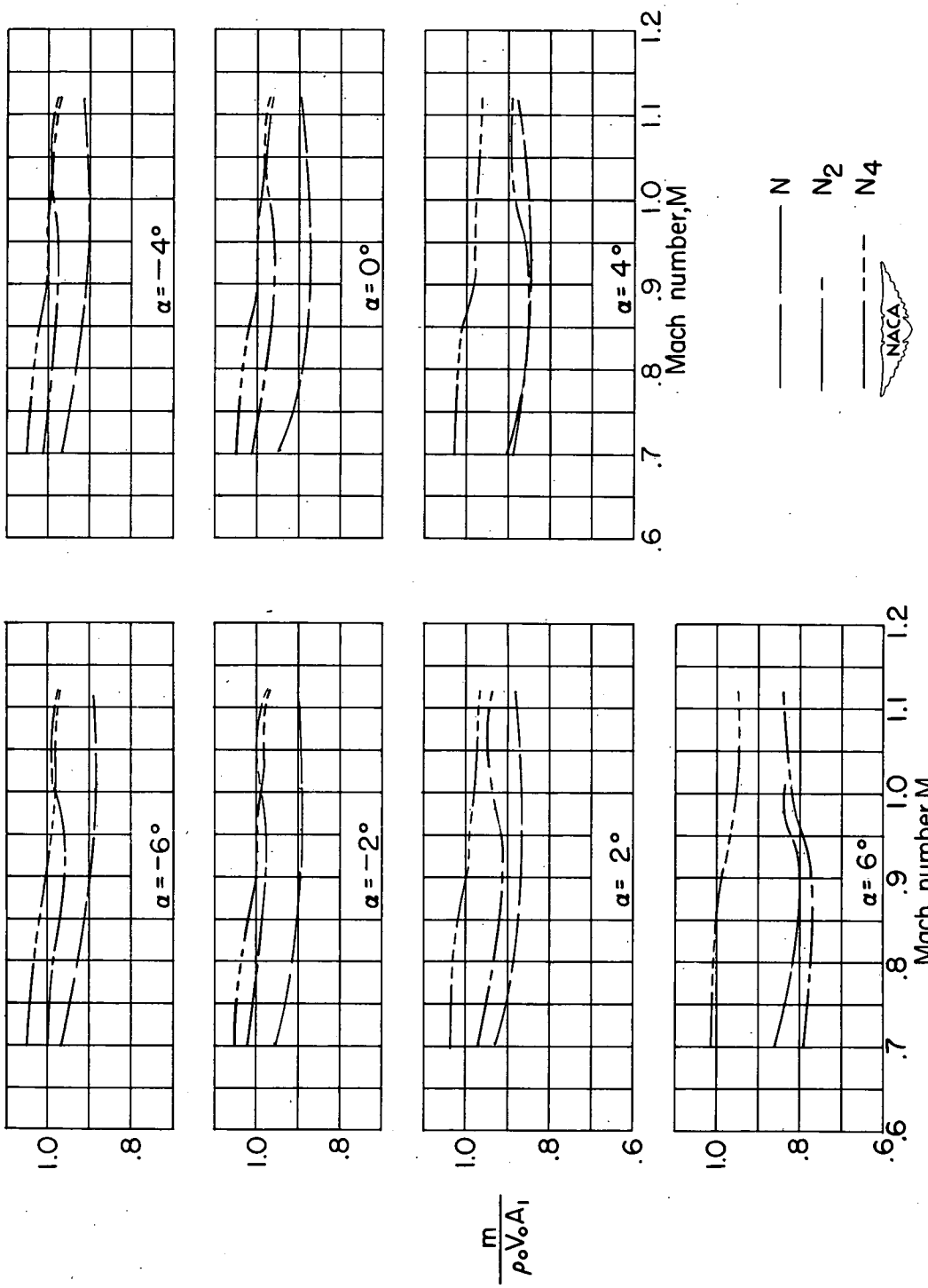

Figure 25.- Variation of mass-flow ratio with Mach number for three of the nacelle configurations investigated.